Hybrid Localization for UAV-based Charging of Wireless Sensor Networks

by

Paul Hamilton Durham

A thesis submitted to the Faculty of Graduate and Postdoctoral Affairs in partial fulfillment of the requirements for the degree of

Master

in

Computer Science

Carleton University
Ottawa, Ontario

Abstract

In Wireless Sensor Networks (WSNs) localization - the assigning of sufficiently accurate positions to nodes - is frequently required to meaningfully identify the data collected. In Wireless Rechargeable Sensor Networks (WRSNs) – in which nodes are recharged by some external energy source – high accuracy (e.g. smaller than the mean internode distance) is often required to enable charging in a reasonably efficient manner with practical charger power.

Localization in Wireless Sensor Networks (WSNs) has attracted research among various strategies, some using Received Signal Strength Indication (RSSI) at nodes. Nodes with known position, called anchors, may be fixed or mobile. Position may be computed by global optimization, or locally between anchors and nodes. For Wireless Rechargeable Sensor Networks (WRSNs), a charger may act as a mobile anchor enabling high-accuracy localization for efficient RF charging.

This study describes a hybrid scheme for localization and charging of WRSNs using an Unmanned Aerial Vehicle (UAV) carrying a node and an RF charger. It works reliably under log-normal fading of RSSI due to shadowing. RSSI localization brings the UAV close enough to the node to elicit a response from the RF charger. The time to charge the node by a given amount is inversely proportional to the power received and thus serves as an indication of proximity of the charger. This metric (ToC) is then used to position the UAV accurately above the node, to allow for charging with maximum efficiency.

Acknowledgements

I would like to thank my advisor, Professor Evangelos Kranakis, for his help and guidance throughout this lengthy endeavour. His support of my original concept, initial references, provision of lab facilities, and suggested improvements through multiple iterations of the text all made possible this finished work.

Thanks to Professor Halim Yanikomeroglu of the Department of Systems and Computer Engineering for his Wireless Seminars, which were a valuable source of ideas.

Finally, I would like to express my appreciation to the faculty at UOttawa's School of Electrical Engineering and Computer Science, and Carleton's Department of Systems and Computer Engineering, who taught all my courses, and to the School of Computer Science and Department of Systems and Computer Engineering for their financial support.

Table of Contents

List of Tables

List of Figures

List of Appendices

Table of Acronyms

dBm – Decibel (milliwatt) – a logarithmic measure of power, equal to $10\log(P/1mW)$

EIRP – Equvalent Isotropic Radiated Power – Transmit power multiplied by antenna gain in the most favoured direction.

GPS – Global Positioning System – a satellite-based system that allows a terrestrial receiver to accurately compute its position based on received signals.

MAN – Mobile Anchor Node - an anchor node for localization of a WSN which moves to various known locations to contribute coordinates to the localization algorithm.

PI – Perpendicular Intersection – a method of estimating node location by using the intersection of perpendiculars, each indicating maximum RSSI on the pass of a mobile anchor.

RSSI – Received SIgnal Strength Indication – a metric of incoming signal strength provided by the receiver of a wireless node.

ToC – Time of Charge – a metric for localization of an RF charged node, which is based on the amount of time needed to charge the node to a useful level.

UAV – Unmanned Aerial Vehicle – a small pilotless aircraft that may be controlled remotely or autonomously, popularly known as a "drone".

WRSN – Wireless Rechargeable Sensor Network - a WSN which is powered from ambient or purposed energy sources such as RF, solar, or mechanical.

WSN – Wireless Sensor Network - a network of small low-powered wireless nodes typically used to monitor environmental or similar data.

Chapter 1: Introduction

Wireless sensor networks (WSNs) consist of many small wireless nodes deployed over an area of interest, monitoring various parameters such as temperature or other atmospheric conditions, biomedical parameters, or industrial parameters. As the nodes are generally not connected to a central power source, energy efficiency is paramount. As a result, the nodes usually transmit with minimum power necessary to obtain a connected network. This results in a network where only nodes within a limited range are connected to each other. This is often modeled by a unit disk graph, which is a graph where nodes are connected if and only if the distance between them does not exceed a fixed distance called the unit disk radius. A WSN routes data to a receiver called a sink which processes and forwards the data. A WSN may have single or multiple sinks which may be either fixed or mobile, however this study simply assumes the existence of a sink or sinks with complete network connectivity.

Most wireless sensor networks require nodes to acquire position coordinates to identify and correlate their data, and for routing. One way to do this is to add a GPS receiver to each node. However, this added hardware entails added cost and power consumption, and may not work in RF sheltered environments.

A great deal of work has been done on localization systems which attempt to calculate location coordinates based on known topology, estimated inter-node distance and angle measurements. Such localization may make use of the known location of anchor nodes to

calculate the location of the other nodes. Anchor-free localization is used in the absence of anchor nodes and results in relative locations.

The more anchor nodes that are available, the more accurate the localization can be made. Instead of using multiple anchor nodes placed in the area, one or more mobile anchor nodes (MAN) may travel around it. This is known as Mobile Anchor Node Assisted Localization (MANAL). MANAL methods may or may not account for the presence of obstacles in the path of the mobile anchor.

Various propagation-related metrics can be used for localization. Received Signal Strength Indication (RSSI) is available for most commercial WSN nodes and can be used to estimate distance but is subject to random error due to fading. Other methods require additional hardware or software resources. Time Difference of Arrival (TDOA) can provide a more accurate estimate but requires precise timer synchronization or different signal propagation (e.g. RF versus ultrasound). Angle of Arrival (AoA) uses angle estimation through beamforming or directional antennas [1].

Algorithms have been developed which perform localization with a suitable degree of accuracy and success for most self-powered WSNs [2]. This study attempts to find an effective method of localization for a movable anchor which also performs RF charging.

1.1 Outline and the Results of the Thesis

A previously implemented co-operative localization package is used to demonstrate the dependence on a high degree of connectivity of the wireless sensor network for accurate localization using fixed anchors. For a small degree of connectivity, the accuracy deteriorates.

The issues facing the use of a UAV acting as both a mobile anchor and RF charger are examined. Efficient RF charging requires a higher accuracy of localization than most other applications. In other approaches, additional localization aids such as optical or ultrasound may be used. In our approach, propagation characteristics are exploited for the use of received signal strength (RSSI) for long and medium range localization, and RF time of charge (ToC) for short range localization to obtain maximum charging efficiency.

An existing mobile anchor algorithm using RSSI triangulation, called perpendicular intersection (PI), is implemented in Matlab with extra steps to provide further refinement using RSSI until ToC localization is feasible. An algorithm for ToC localization is implemented which performs a stepwise reduction of the charging feasible area until 90% of maximum power is achieved. The PI algorithm is then extended to perform more efficient traversals of the wireless sensor field with fewer turns, and to make use of multiple RSSI traces which result in multiple location estimates, as opposed to the single estimate produced by the original PI. The number of estimates to be visited is reduced, when possible, by a disk cover reduction algorithm.

These algorithms are then tested with charger effective isotropic radiated power (EIRP) of 4W and 160W. 4W is the highest EIRP allowed for unlicensed use and so is appropriate for use together with unlicensed WSN technologies. Using a smaller power offers no

advantages as it would reduce the charging footprint radius to less than the effective RSSI location radius at the cost of more UAV movement and would not reduce total charging energy (see Analysis of Geometry for UAV Based Mobile Anchor and Charger). 160W was chosen for comparison to 4W as it results in a charging footprint with twice the radius. It is found that the extended PI algorithm using equilateral triangulation (extending the original PI) is the most effective at obtaining an estimate within the charging footprint with the shortest localization trajectory. An extended PI algorithm using side-to-side isosceles triangulation is found to be the least effective due to the sub-optimal angles of the resulting perpendiculars. Surprisingly, a charger power of 160W is found to be less effective than 4W. Thus, the extended PI algorithm is shown to be effective for enabling RF charging at the lower power.

Chapter 2: Related Work

2.1 Cooperative Localization

Cooperative localization schemes acquire the internode distance estimates, e.g. based on the RSSI values for every pair of connected nodes, and locations of known anchor positions, and assign positions to nodes by solving an optimization problem which tries to minimize some error function (e.g. total error of computed internode distance versus observed "noisy" distance) over the network. It can obtain good results for most nodes given suitable values for number of anchors and average degree of the connectivity graph.

Obstacles will often be present between nodes. This brings about variation in the received signal strength, i.e. fading. There are various probability distributions used to model fading. In the case of obstructions without significant reflections, i.e. shadowing, the log-normal distribution is commonly used. In a log-normal distribution, the logarithm of the random variable observes a normal distribution. This can be expressed concisely as:

$$P_r[dBm] = \overline{P_r} + X_\sigma \quad (1)$$

Here $P_r[dBm]$ is received power in dBm, $\overline{P_r}$ is mean power level in dBm, and X_σ is a normally distributed zero mean Gaussian random variable with standard deviation σ in decibels.

If the RSSI value is log-normally distributed, the internode distance estimates will be log-normally distributed as well:

$$P_r = P_t\, G_t G_R (\lambda/4\pi d_{est})^2 10^{0.1X_\sigma} \quad (2)$$

$$d_{est}^2 = (P_t\,/P_r\,) G_t G_R (\lambda/4\pi)^2\; 10^{0.1X_\sigma}$$

$$2\log d_{est} = \log(P_t\,/P_r\,) G_t G_R (\lambda/4\pi)^2 + 0.1X_\sigma$$

$$\log d_{est} = \log(P_t\,/P_r\,) G_t G_R (\lambda/4\pi)^2 + 0.05X_\sigma$$

where:

d_{est} is the estimated distance.

P_r is the measured signal power at the receiver.

P_t is the known signal power at the transmitter.

G_t is the known antenna gain at the transmitter.

G_r is the known antenna gain at the receiver.

λ is the wavelength of the signal, i.e. the speed of light divided by the frequency.

X_σ is the standard deviation of the log-normal fading as described previously.

The Cramer-Rao bound (CRB) provides a lower bound on the error of the localization [3]. The localization algorithm may be distributed among the nodes or performed at a central site. However, the computing requirements are substantial and may exceed the capabilities of hardware deployed in the field. An example of central site global optimization using semidefinite programming can be found in [4]. Related Matlab code modules which were used to support this study were obtained from the website [5].

2.2 Mobile Anchor Node Assisted Localization [MANAL]

The variance in RSSI for a given distance described above can cause significant inaccuracy in localization algorithms which depend on a single RSSI reading between two given nodes. Localization can be made more robust by using a mobile anchor to obtain a series of RSSI readings for a given node [2]. Computation of estimated position can then be done locally, i.e. for each node without reference to other nodes. Also, substantially fewer computing resources are required compared to a global optimization, and on-demand localization is facilitated.

Rather than computing multiple distance estimates from these readings, the point of maximum proximity on the trajectory may be computed. One useful algorithm, known as Perpendicular Intersection or PI, obtains the maximum reading for RSSI along a linear trajectory within the maximum transmission radius [6]. A perpendicular line at the point of maximum RSSI will point toward the node. Using a running average of RSSI values increases the likelihood of the perpendicular being located near the actual point normal to the node.

2.3 Perpendicular Intersection (original) MANAL

Using two trajectories at an angle, e.g. two sides of an equilateral triangle, will obtain an intersection of perpendiculars which estimates the node location, as shown in Figure 1. Starting at P_1 at (x_1, y_1) the mobile beacon moves to P_2 at (x_2, y_2) sending out hellos to node *N* at (x, y) at a rate of 20 per triangle edge, which is equal in length to the transmission radius. The highest RSSI is received at point *A* at (x', y') which is closest to the node *N*. The mobile beacon then turns and moves from P_2 to P_3 at (x_3, y_3) again sending out hellos. The highest RSSI is received at point *B* (x'', y''). The intersection of the perpendiculars from *A* and *B* indicates the estimated location of *N*. This estimate can be computed using simple matrix operations.

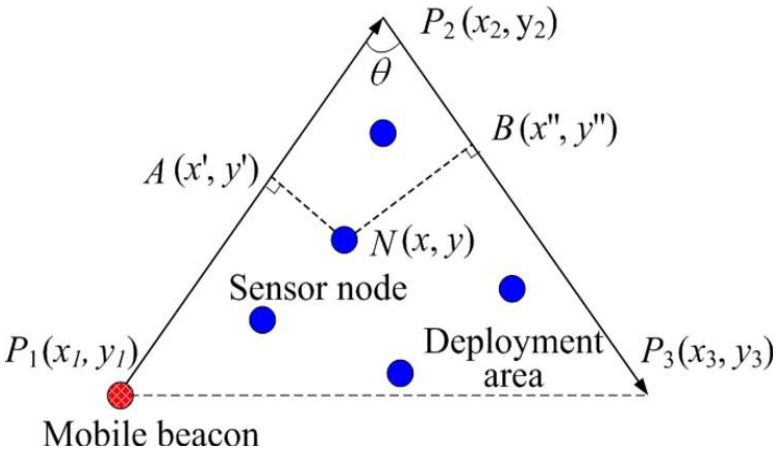

Figure 1 - Perpendicular Intersection Localization of triangle P_1-P_2-P_3 [6]

To locate all the nodes in the deployment field requires tiling the field with triangles. A path traversing two sides of each triangle in sequence will be in range of all nodes in its interior. However, it requires two turns for each triangle, thus the number of turns is proportional to the area of the field divided by area of the triangle, which equals the square of the side of the field divided by the transmission radius. This turning of the

mobile anchor is costly in terms of time and energy. In addition, a turn at each vertex of the triangle ends the data collection for nodes in its interior while nodes closer than the opposite vertex are still in range. This loss of additional data points reduces the potential accuracy of the localization.

The tiling of a field of width L and height H is illustrated in Figure 2.

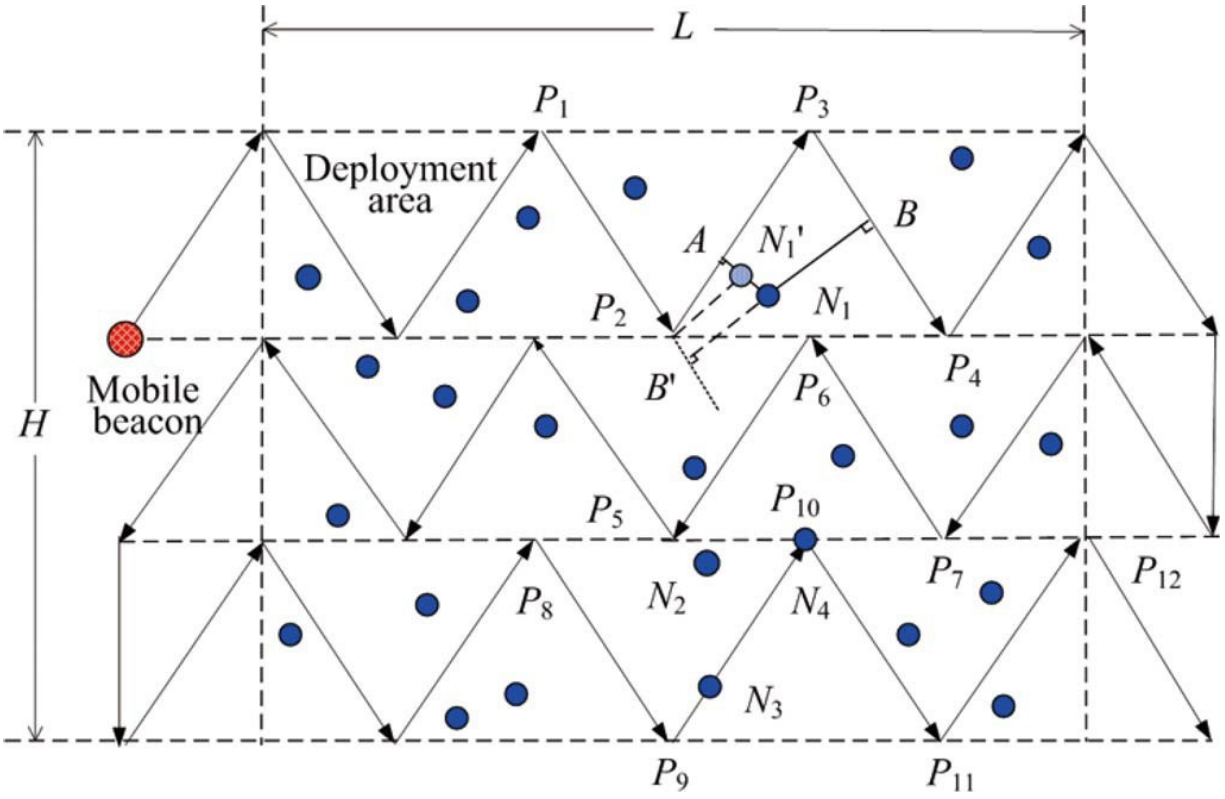

Figure 2 - Perpendicular Intersection Tiling of WSN Field [6]

However, by making turns only at the boundaries of the WSN field, the same area can be covered with the number of turns proportional to the side of the field divided by the transmission radius. This can reduce travel time and energy required by the mobile anchor. As well, data points are not lost while any node is still in range. This approach is developed below in section 3.2 - Augmented PI Traversal.

2.4 RF Charging Considerations

Much work has been done regarding the use of RF energy harvesting to fully or partially power WSNs. Such networks are known as Wireless Rechargeable Sensor Networks (WSRNs). Using available components, a received power on the order of 1mW, i.e. 0 dBm, is generally required at the node to usefully harvest RE energy. This may be provided by a very high-power source, e.g. a TV transmitter, at a distance on the scale of kilometres, or by a fixed or mobile power source at lower power and a much closer distance. Harvested energy made be stored at the node by a supercapacitor, a rechargeable battery such as nickel metal hydride, or a combination of the two based on power requirements and charging cycle times [7].

An example of a RF-powered sensor is the Wireless Identification and Sensing Platform (WISP), which combines RFID identification with sensor functions [8]. It is designed to use RFID reader transmitting in the 910 MHz range as a charger. Such a device could use the RFID reply to indicate proximity to the charger, and then receive energy for subsequent sensor operation after the charger has moved away.

The WISP module cited above can respond to a minimum received RF power level of -9.5 dBm. Using a mobile RF charger at practical power levels, e.g. EIRP of 4 watts, at an altitude on the order of 1.0 metre requires the estimated distance between node and charger to have an accuracy on the order of 1.0 metre to elicit a response to the charger from the node.

2.5 Time of Charge Localization for WRSN

If a path can be traversed that puts the nodes within the effective range of a charger-equipped mobile anchor, the Time of Charge (ToC) measurement may be used by a localization algorithm [9]. This is the amount of time needed to charge the node to a level which elicits a response. The smaller the time, the higher the charging power received. If the terrain is suitable it may be possible to perform ToC localization alone using a ground based mobile charger with vertical antenna, i.e. transmitting horizontally, since its own location can be tracked exactly though wheel rotations. On the other hand, as noted above an Unmanned Aerial Vehicle (UAV) transmitting vertically will have a limited charging footprint, i.e. the area in which the charging power is usable and will usually not be able to track its position with sufficient accuracy.

This may be addressed using an optical, ultrasound or radar guidance system with added hardware and resource costs [10]. Without such a system it may be possible to use mobile anchor based RSSI localization to obtain an initial estimate which has a reasonable probability of being within the charging footprint.

Chapter 3: Localization for UAV Charging

The use of a mobile anchor combined with RF charger implemented on an aerial platform presents a distinctive set of issues elaborated below.

3.1 Propagation Issues for UAV Localization

Most localization schemes assume that the nodes reside in a plane, i.e. in two dimensions. There are also schemes for localization of three-dimensional WANs. Special cases also exist, i.e. where the nodes reside in a plane and the anchors travel in three dimensions, or in another plane. It may be necessary for the MAN to travel in another plane when the plane where the nodes reside contains obstacles which make ground level movement by a MAN difficult.

In the case at hand we consider nodes residing in a single plane, with a single mobile anchor travelling in another plane. This is the situation to be found where a UAV (Unmanned Aerial Vehicle, aka drone) carrying a node is used as a mobile anchor. A UAV approaching a node over an obstacle is shown in Figure 3.

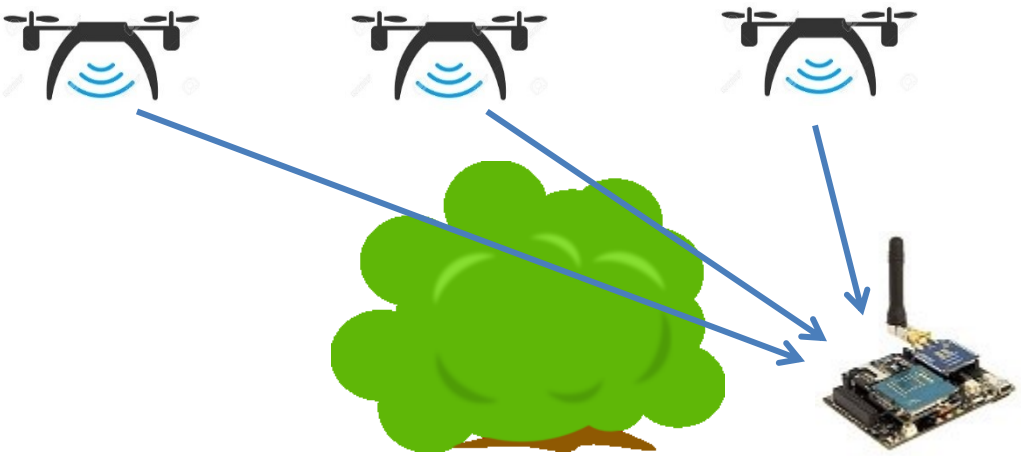

Figure 3 - Shadowing of UAV above WSN

As shown above, obstacles may partially or fully obscure the line of sight between a MAN and a node. This brings about variation in the received signal strength, i.e. fading. As previously noted, the log-normal distribution is commonly used to model fading due to obstructions:

$$P_r[dBm] = \overline{P_r} + X_\sigma \tag{3}$$

In this case the standard deviation σ will depend on the density of obstacles, and the angle of attack of the UAV. The higher the angle of attack, the less likely the path will be obscured. This means that the closer that the UAV approaches the node the smaller the standard deviation of the fading.

3.2 Augmented PI Traversal

The previously cited PI algorithm does not collect all available RSSI information as it localizes nodes within only one triangle at a time. An edge to edge trajectory, herein called augmented PI, can obtain all RSSI information up to the maximum transmission distance resulting in improved accuracy. As well.by turning only at the edges of the field turn overhead is greatly reduced. In Figure 4 the green dashed lines illustrate the potential RSSI data points in range of node *N*. This data set is truncated by the original PI trajectory (in black) but collected in full by the augmented PI trajectory (in blue).

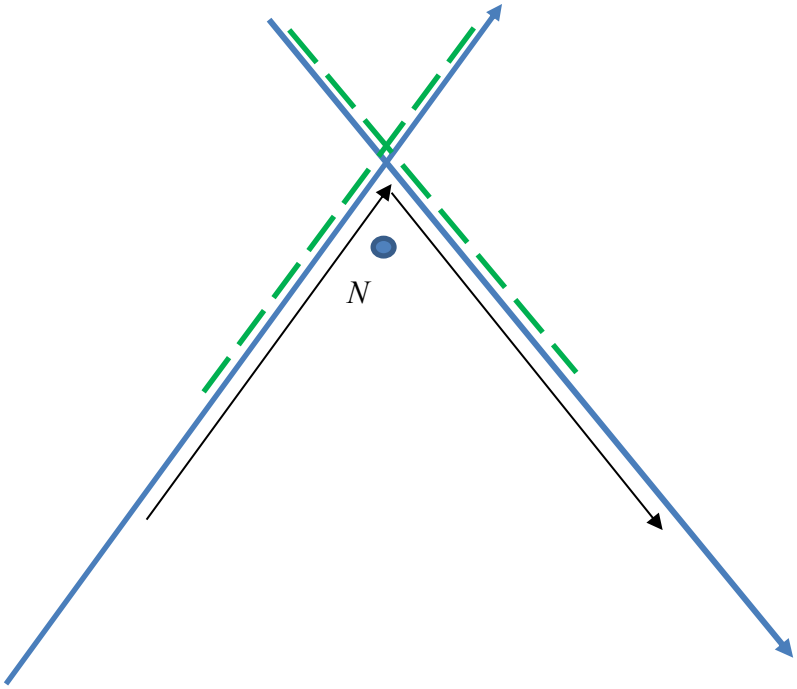

Figure 4 - RSSI node coverage for original versus extended PI

Unlike the sequential tiled traversal of original PI, many triangles are traversed with the two sides out of sequence. This means that nodes, or the MAN, need to store RSSI

sequences for future use. The trajectory must cover the sensor area with each sensor within transmission radius of at least two passes.

Two edge to edge trajectories are examined here. The first covers the sensor field with equilateral triangles with side equal to the transmission radius, like the original PI. The second covers the sensor field with isosceles triangles with base equal to twice the transmission radius resulting in shorter traversal and fewer turns. Testing will show which edge to edge trajectory is most effective overall.

3.3 Non-oblivious Localization

Most localization algorithms try to localize all nodes ahead of any demands to know their location which results in a fixed trajectory such as the tiling trajectory above. Non-oblivious localization uses previously collected partial information to aid the localization of nodes upon demand. In our scheme the first estimate of location is made from RSSI during the initial trajectory and then refined from ToC when a node requires charging. Due to uncertainly in positioning further refinements may be made on subsequent returns.

In addition, if the angle of approach to a node is similar to that of the original trajectory, more RRSI traces are collected for nodes within range.

3.4 Reducing the Number of Traces used for Localization Estimates

The extended traversals will produce multiple up and down RSSI traces for most nodes. Given *m* up traces and *n* down traces, this will yield $m \times n$ intersections of perpendiculars and thus $m \times n$ localization estimates. To reduce the amount of travel, inferior estimates are reduced by the following strategies:

1. RSSI traces which are shorter than the side of the original triangulation are discarded.
2. RSSI traces which are unbalanced, i.e. the maximum RSSI is within ¼ of the trace from either end, are discarded.

The estimate derived from the longest up and down RSSI traces is denoted the "first" estimate as it is the first visited by the UAV.

3.5 Reducing the Number of Localization Estimates Visited

The ToC coverage of RSSI localization estimates may overlap to the extent that only a subset needs to be visited to cover the same area. Finding the minimal subset is an instance of the Minimal Unit Disk Coverage Problem (MUDCP) which is a special case of the Minimal Set Coverage Problem (MSCP). MSCP is NP-complete, and it has been shown that MUDCP is NP-complete as well [11]. Thus, computing an exact solution is impractical.

However, a less exact reduction can be computed in $O(n^2)$ time by using the sponsored sector algorithm to identify disks which are completely covered by their neighbours. If two disks with the same radius intersect, and the distance between them is less than the radius, the area of intersection contains a sector defined by the centre of the disk, and the intersections of the circumferences.

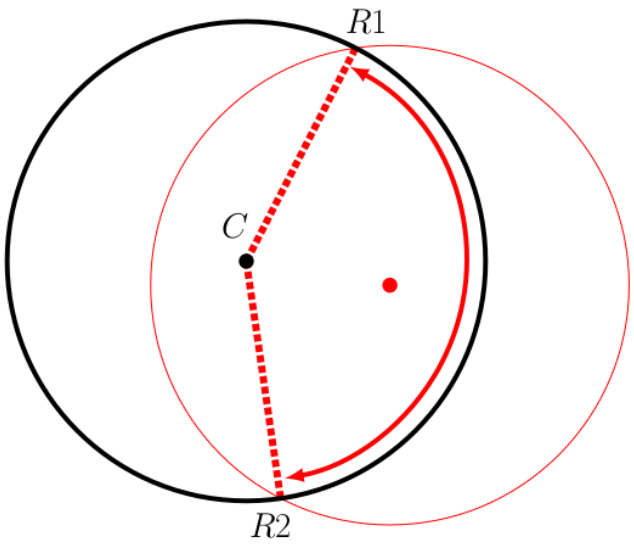

Figure 5 - Sponsored Sector Definition

Theorem: Given a disk D of radius r, and a set of disks S each with centre to centre distance from D <= r, if the entire circumference of D is covered by S, then D is covered by S.

Proof: Refer to Figure 5. Let D be the black disk centred at C. Since the disks are convex, the sector *R1-C-R2* lies within the intersection of the red disk with D. If all of the circumference of D is covered by the set of disks, the union of sectors so defined will equal D as every point on its circumference with be on the edge of at least one of the sectors.

If the union of all such sectors equals a disk, that disk can be eliminated without affecting coverage, i.e. the union of all the disks remains the same [12]. It can be seen in Figure 6 that the angles *B1-C-B2*, *G1-C-G2*, and *R1-C-R2* cover the circumference of the black disk completely, thus the black disk is covered by the blue, green and red disks.

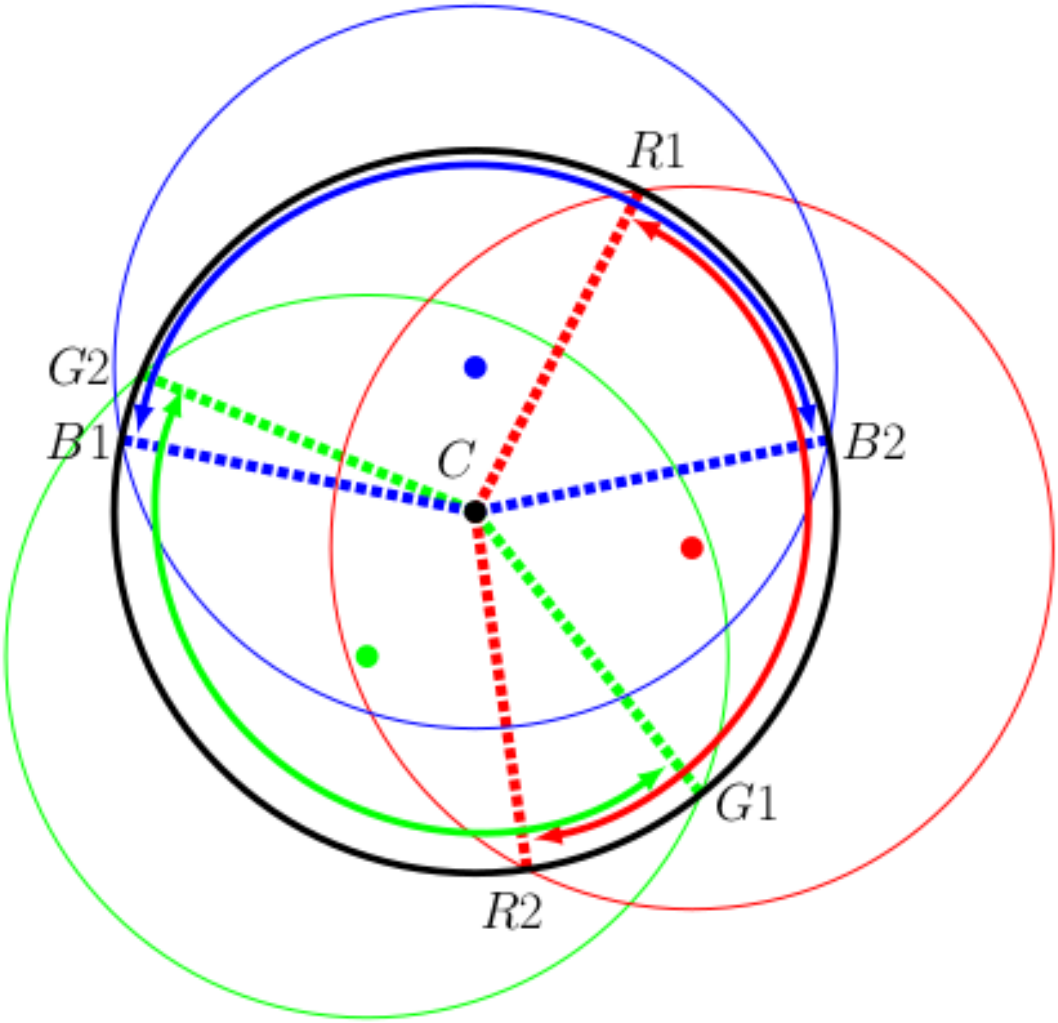

Figure 6 - Sponsored Sector Coverage of Disk

To verify full coverage, first calculate the angle of the central radius (relative to the positive x axis) and the span of each sector from the circumference intersection points. Then order the sectors by the angle of the central radius, i.e. in a counterclockwise direction. Consolidate the first sector with the second. If there is a gap, coverage fails. Repeat until only one sector remains. If this covers the full disk, coverage succeeds.

Algorithm 1: disk cover reduction algorithm

input : set of disks $d_i \in Din$, defined by centre (x_i, y_i), all with radius r

output: set of disks $Dout \subseteq Din$, such that $\cup\{d|d \in Din\} = \cup\{d|d \in Dout\}$

Result: disks completely covered by neighbours are removed

```
put disk parameters in an array;
sort array by distance of centre from first estimate;
currentdisk = last disk in array;
while currentdisk != first disk in array do
    for all disks centred less than r from currentdisk do
        compute circumference intersection points with
         currentdisk;
        compute angles of central radius and intersection points
         for covered sector;
        add central angle and span for covered sector in
         currentdisk to sector array;
    end
    sort sector array by central angle;
    consolidate sectors;
    if consolidated sectors cover currentdisk then
        remove currentdisk from disk array;
    end
    currentdisk = previous disk in array;
end
```

Figure 7 - Disk Cover Reduction Algorithm

A sample input and output of the algorithm coded in Matlab is shown below.

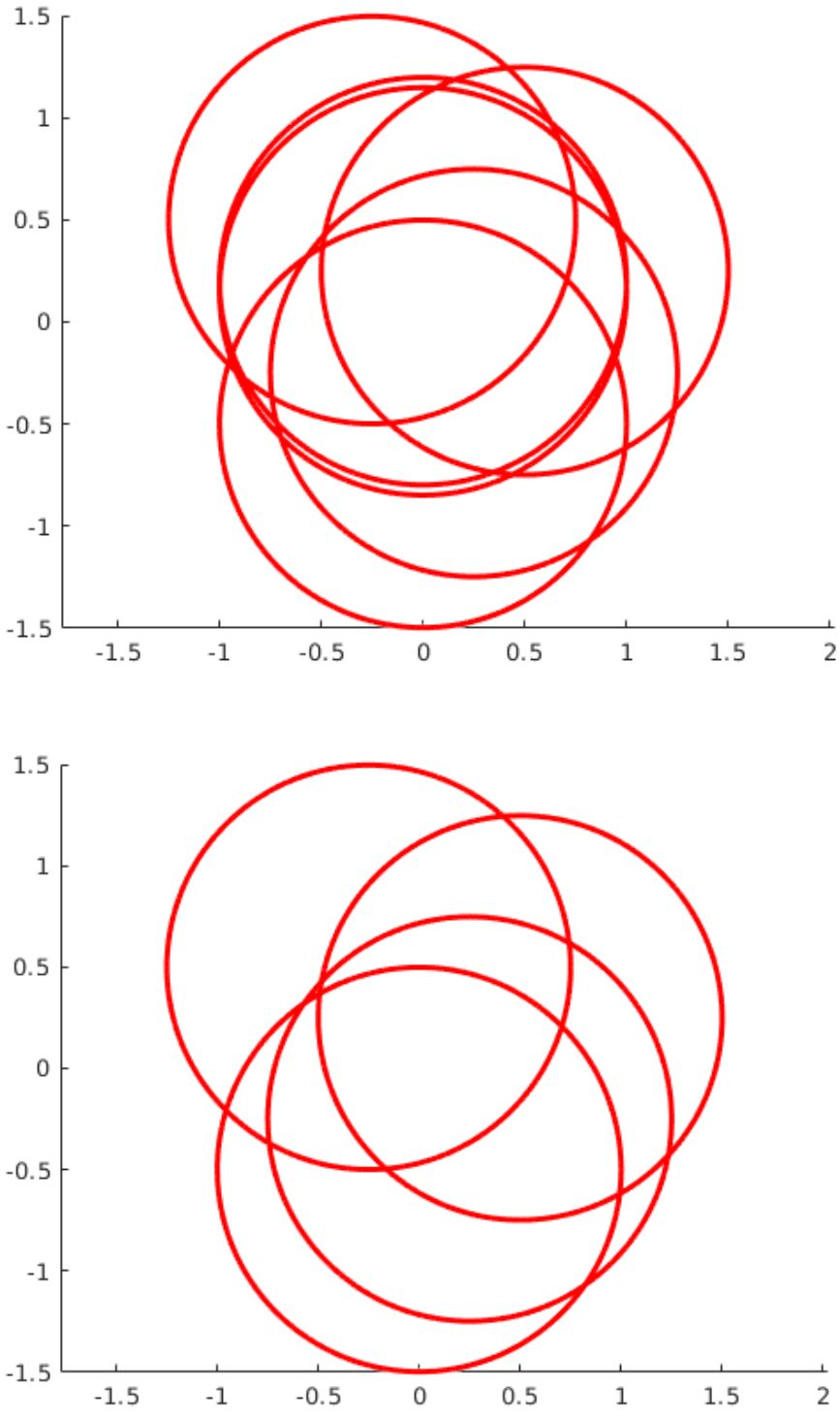

Figure 8 - Disk Cover Reduction Example (Matlab)

3.6 RSSI Localization Refinement

Localization using a trajectory length equal to the transmission radius often will not be accurate enough to fall into the charging footprint as described below. As well in some situations the nodes may move from previously located positions. For these reasons when the UAV seeks to charge a node and finds it out of range it will refine the position using a smaller RSSI trajectory length on a full triangle. This produces three perpendicular intersections, the average of which provide a more accurate localization. The UAV can test whether it is in the charging footprint be issuing a probing charge and listening for a reply from the backscatter transmitter in the node's charging unit. If the UAV is not within the footprint, a further refinement can be performed with a smaller radius until it is found. The smallest radius that is useful is where the RSSI function reaches its maximum. If this is reached without the changing footprint being found, the RSSI localization has failed and a spiral search is performed for the charging footprint.

3.7 ToC Refinement

Once the UAV has been established to be in the charging footprint, it can be positioned precisely by division of the feasible area. By alternately moving the x and y positions and selecting the position with the smallest time of charge, i.e. the largest received charging power, the feasible area may be reduced in each step. The algorithm completes when it achieves at least 90% of full charging power, i.e. where the UAV is effectively directly above the node.

At the initial position of the UAV the feasible area is circular, i.e. lying within a fixed radius of the point below the UAV. However, the positioning algorithm assumes a rectangular feasible area for simplicity. At each step it chooses between three positions,

thus dividing the feasible area into three parts. The feasible area is then reduced to the part containing the position resulting in the highest charging power.

The probability a given location being within the feasible area is

$$p_i = \frac{A_{0.90}}{A_i} \tag{4}$$

Where $A_{0.90}$ is the area where the power level is within 90% of maximum, and A_i is the area of the current feasible area at step *i*, which is divided by 3 at each step. Thus, the sequence will have at most *n* steps, where

$$n = \left\lceil \log_3 \left(\frac{A_0}{A_{0.90}} \right) \right\rceil \tag{5}$$

The expected value of the number of steps *S* is

$$E[S] = \sum_{k=0}^{n} p_k \times k \tag{6}$$

In Figure 9 below, the feasible area is coloured blue. 1, 2, 3 represent the level of received charging power at the different UAV positions, 1 (yellow) being the strongest and 3 being the weakest.

A: Move to left and right of feasible area. Reduce feasible area to leftmost 1/3
B: Move to top and bottom of feasible area. Reduce feasible area to top 1/3
C: Move to left and right of feasible area. Reduce feasible area to middle 1/3
D; Move to top and bottom of feasible area. Reduce feasible area to bottom 1/3

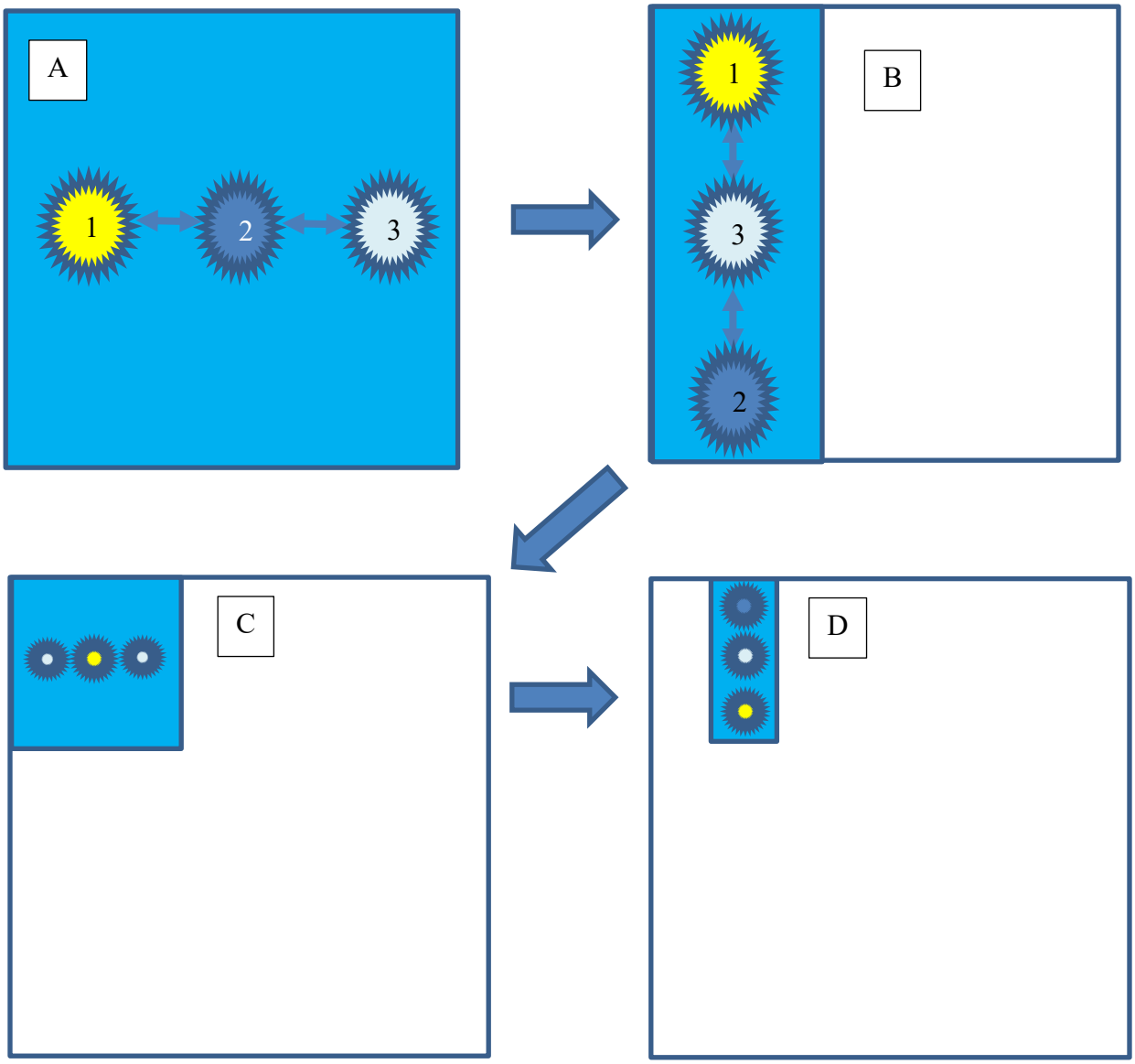

Figure 9 - Stepwise Refinement of UAV Position using ToC

3.8 Analysis of Geometry for UAV Based Mobile Anchor and Charger

The UAV is modeled as carrying a node operating in the 2.4 GHz band and a charger operating in the 910 MHz band. The WSN nodes operating in the 2.4 GHz band will be augmented with a backscatter RFID transceiver operating in the 910 MHz band, serving as a charging controller. WSN nodes commonly use vertical antennas which are omnidirectional in the horizontal plane. For the analysis I assume a ¼ wavelength vertically polarized antenna with reflector which has a closed form expression for its vertical pattern, i.e. $\sin^2(\theta)$ with a maximum gain normal to the antenna as shown in Figure 10. Since it radiates into only half of free space, this gain will be twice the ½ wave dipole's gain of 1.64 or 2.15 dBi, i.e. 3.28 or 5.15 dBi [13]. Other vertical antennas may be used in actual implementations but providing the antenna pattern has a single node the RSSI function will take the same shape. The charger has a horizontally polarized antenna with reflector (maximum down) and the power controller has a horizontally polarized antenna with reflector (maximum up) with the same gain as the vertical antennas. Problems with radial alignment can be avoided by using circular polarization. For illustration I have calculated the charging signal strength assuming a $\cos^2(\theta)$ pattern as shown in Figure 11.

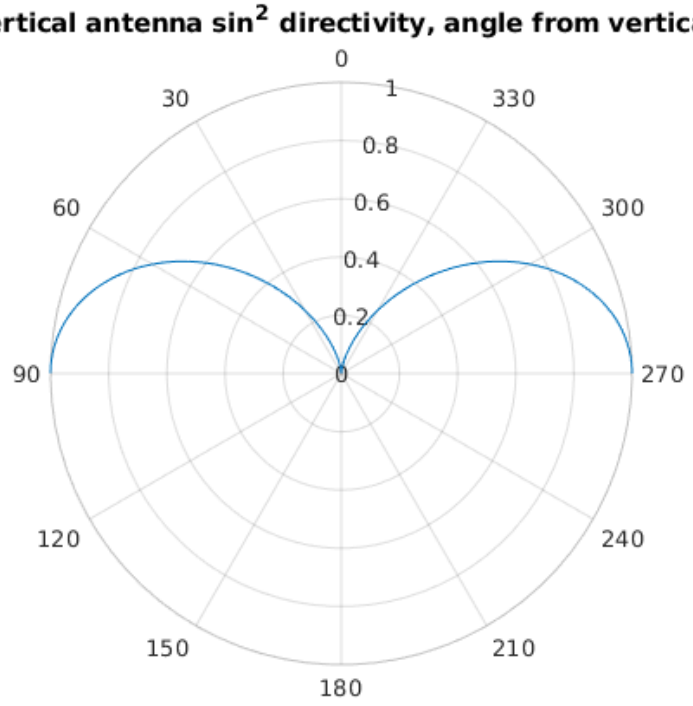

Figure 10 - Directivity of Vertical Antenna with Reflector

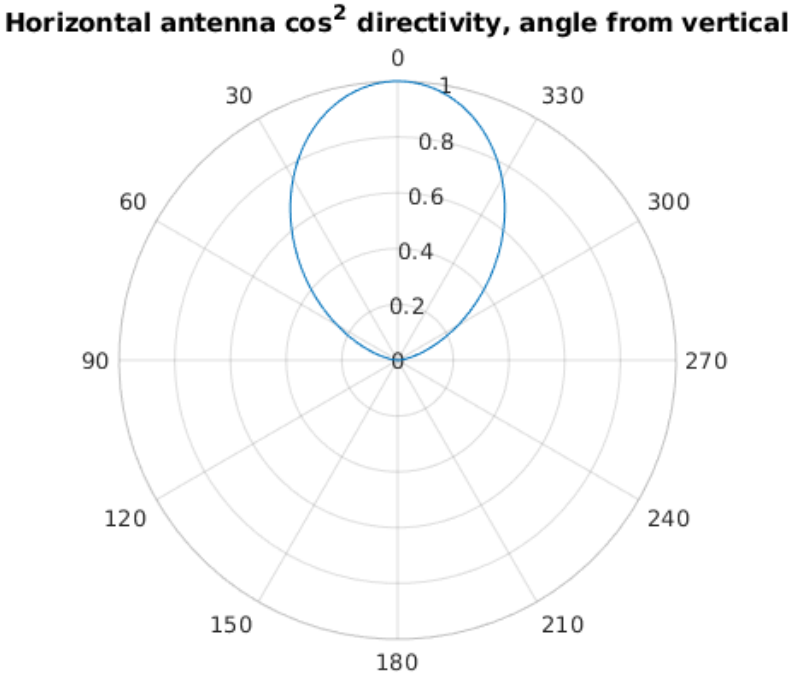

Figure 11 - Directivity of Horizontal Antenna with Reflector

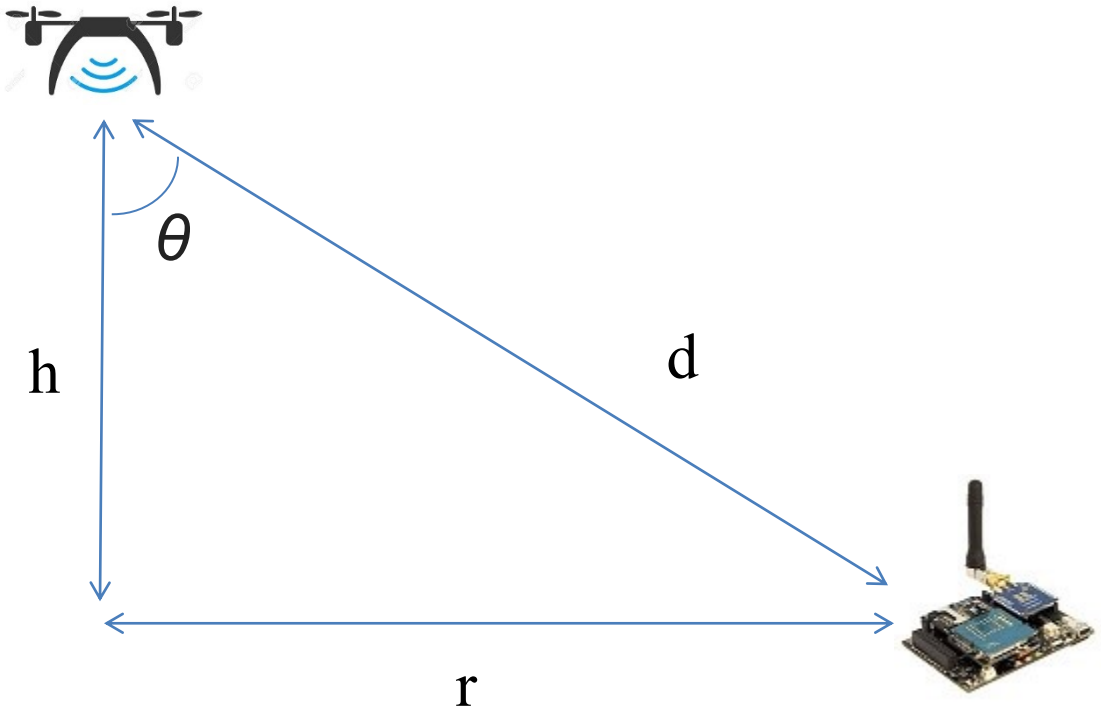

Figure 12 - Geometry of UAV above Sensor Node

In Figure 12 *r* is the horizontal radius from UAV to node, *h* is the UAV elevation, and *d* is the total distance. It can be seen that

$$d^2 = r^2 + h^2 \tag{6}$$

$$\sin^2\theta = \frac{r^2}{d^2} \tag{7}$$

$$cos^2\theta = \frac{h^2}{d^2} \tag{9}$$

Using the Friis transmission formula [14]

$$P_r = P_t \; G_r \, G_t \, \frac{\lambda^2}{(4\pi d)^2} \tag{10}$$

And the vertical antenna pattern from Figure 10

$$G_r = G_{r_0} \sin^2\theta \tag{11}$$

$$G_t = G_{t_0} \sin^2\theta \tag{12}$$

We obtain the following:

$$P_r = P_t\, G_{t_0}\, \sin^2\theta\, G_{r_0} \sin^2\theta\, \frac{\lambda^2}{(4\pi d)^2}$$

$$= P_t\, G_{t_0}\, G_{r_0} \sin^4\theta\, \frac{\lambda^2}{(4\pi d)^2}$$

$$= P_t\, G_{t_0}\, G_{r_0} \left(\frac{r}{d}\right)^4 \frac{\lambda^2}{(4\pi d)^2}$$

$$= P_t\, G_{t_0}\, G_{r_0} \frac{r^4}{(r^2+h^2)^2}\, \frac{\lambda^2}{16\pi^2(r^2+h^2)}$$

$$= P_t\, G_{t_0}\, G_{r_0} \frac{r^4}{(r^2+h^2)^3}\, \frac{\lambda^2}{16\pi^2} \qquad (13)$$

Figure 13 illustrates that as r approaches ∞, P_r approaches 0. As r approaches 0, P_r also approaches 0. Maximum P_r is at $r^2 = 2 * h^2$, i.e.

$$r = \sqrt{2 * h^2} = \sqrt{2} * h \qquad (14)$$

.

Similarly using the horizontal antenna pattern from Figure 11

$$G_r = G_{r_0} \cos^2 \theta \tag{15}$$

$$G_t = G_{t_0} \cos^2 \theta \tag{16}$$

we obtain

$$\begin{aligned} P_r &= P_t \, G_{t_0} \, \cos^2 \theta \, G_{r_0} \cos^2 \theta \, \frac{\lambda^2}{(4\pi d)^2} \\ &= P_t \, G_{t_0} \, G_{r_0} \cos^4 \theta \, \frac{\lambda^2}{(4\pi d)^2} \\ &= P_t \, G_{t_0} \, G_{r_0} (1 - \sin^2 \theta)^2 \, \frac{\lambda^2}{(4\pi d)^2} \\ &= P_t \, G_{t_0} \, G_{r_0} \left(1 - \frac{r^2}{(r^2 + h^2)^2}\right)^2 \frac{\lambda^2}{16\pi^2 (r^2 + h^2)} \end{aligned} \tag{17}$$

Figure 14 illustrates that the received power is strictly decreasing with increasing *r*.

In the simulations G_{t_0} and G_{r_0} are assumed to be that of the ¼ wave with reflector, i.e. 3.28 or 5.15 dBi.

With the UAV closer than $\sqrt{2} * h$, RSSI declines with decreasing r and reaches zero directly above the node as the antennas are end-to-end. In practice factors such as vertical misalignment and reflections will obscure this effect. Thus, the RSSI pattern within this radius cannot be depended on to guide localization and this radius should exceed the radius of the charging footprint.

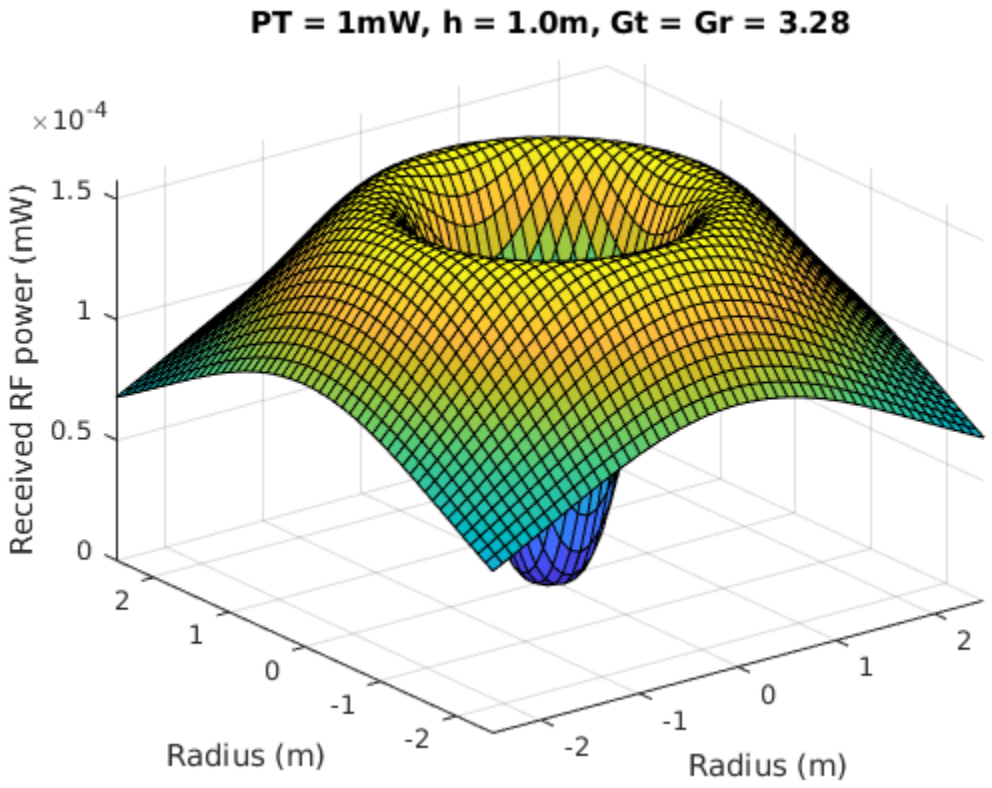

Figure 13 - RSSI from UAV at Sensor Node

The area of decreasing RSSI with decreasing radius lies within the effective charging footprint at 4W EIRP charging power as shown in Figure 15. This enables a multi-step localization strategy using RSSI and ToC. The UAV will obtain an estimate (original PI) or estimates (augmented PI) of its proximity to the target node through RSSI. This will be refined if outside the charging footprint by traversing an extra triangle. Once close enough, ToC will be used to locate the optimal position for charging. Both methods need to be adapted to the UAV-network geometry as described above.

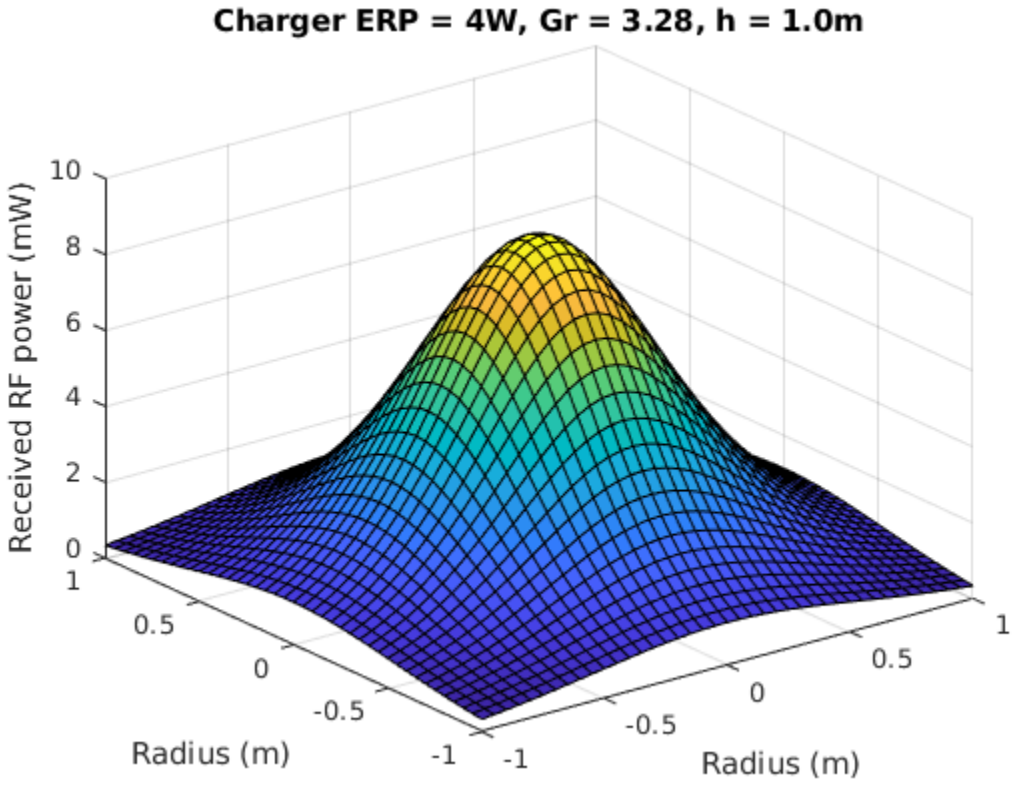

Figure 14 - Received Charging Power from UAV at Sensor Node

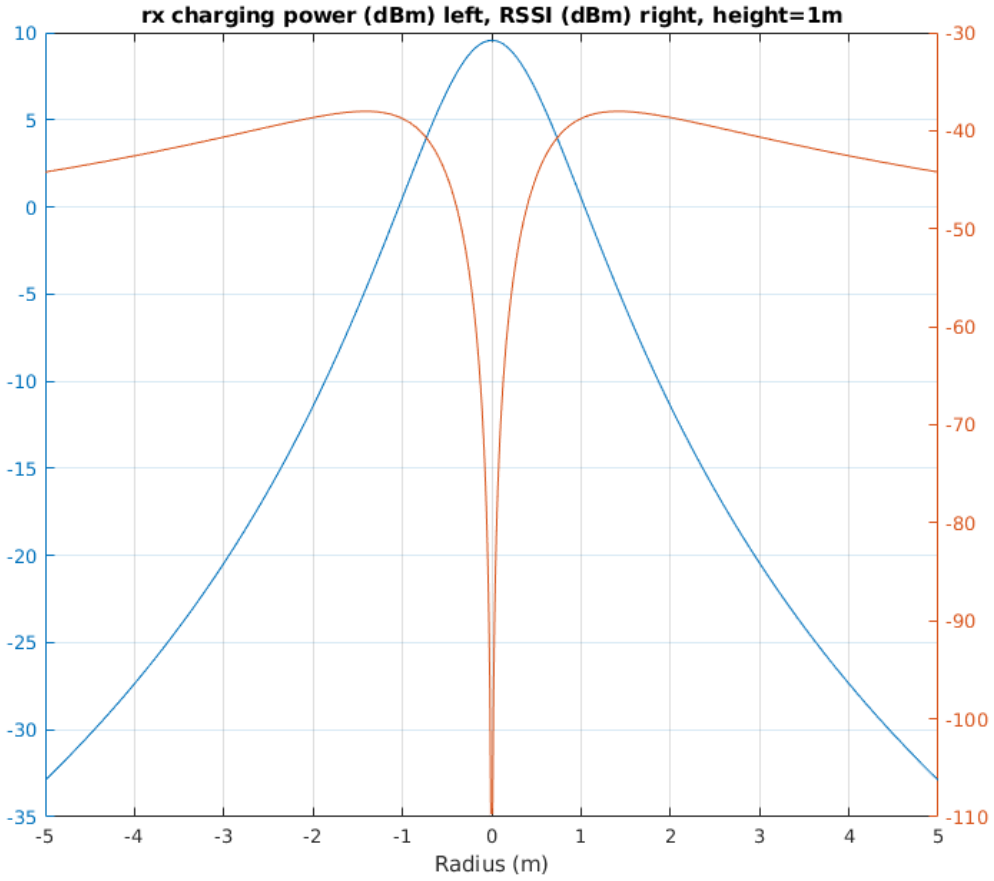

Figure 15 - RSSI versus Charging Power at Sensor Node, Charger EIRP=4W

Chapter 4: Simulations

Simulations were performed using a field of 100 sensors with positions following a two-dimensional Poisson distribution. The position data files were as supplied with the Semidefinite Programming package [5].

To obtain comparative results for cooperative localization with fixed anchors, the Semidefinite Programming package was used.

Three mobile anchor triangulation schemes were implemented. The basic Perpendicular Intersection algorithm was coded in Matlab. The augmented Perpendicular Intersection algorithm was implemented in two variants, one using edge to edge traversal to produce an equilateral triangle tiling similar to the original Perpendicular Intersection, and the other using edge to edge traversal to produce an isosceles triangle tiling. In addition to the MATLAB code they use node objects coded in Java to support the extended trace information. More than two traces may be available for a given node and are used for localization. All triangulations assume a transmission radius (referenced as u) of 0.2 relative to the field size of 1.0, which models 20 metres versus 100 metres.

The initial localization for each node is then tested by moving the UAV to its coordinates and attempting to elicit a charging response. If it is found the ToC refinement obtains localization to the desired accuracy. If not, an additional triangulation is performed, and the result is again tested against ToC. If this fails a spiral is performed until the node is found. This is a last resort and indicates a failure of the localization to obtain the needed accuracy.

4.1 Rationales

The Semidefinite programming package was chosen to illustrate the weakness of RSSI-based cooperative localization with fixed anchors in a WSN with log-normal fading and a small transmission radius relative to field size. No charging is attempted.

The original Perpendicular Intersection algorithm with equilateral tiling was implemented with added refinement to illustrate an effective strategy for mobile anchor RSSI-based localization and subsequent ToC localization.

The augmented Perpendicular Intersection algorithm with equilateral tiling was implemented to illustrate that including RSSI data points missed by the original PI algorithm and enabling multiple estimates results in more accurate localization.

The augmented Perpendicular Intersection algorithm with isosceles tiling was implemented to investigate the how a strategy of reducing trajectory length and number of turns would affect location accuracy.

The 4W charging power was chosen as it is allowed for unlicensed use. Lower charging power would result in a charging footprint too small to be effectively located using RSSI as can be seen from Figure 15 - RSSI versus Charging Power at Sensor Node, Charger EIRP=4W, and preceding text. The 160W charging power was chosen to illustrate the effects of doubling the charging footprint radius from 4W.

4.2 Semidefinite Programming

This package is as described in [4]. Five anchor points were used (shown as diamonds). The green circles represent the actual node positions and the red asterisks the estimated positions. To obtain accurate localization the connectivity graph must have a high average degree, i.e. the sensors must densely populate the field to obtain adequate distance estimates. With a transmission radius of 0.5 and a density of 100, average degree is 7. As shown in Figure 16, localization accuracy is good for most nodes.

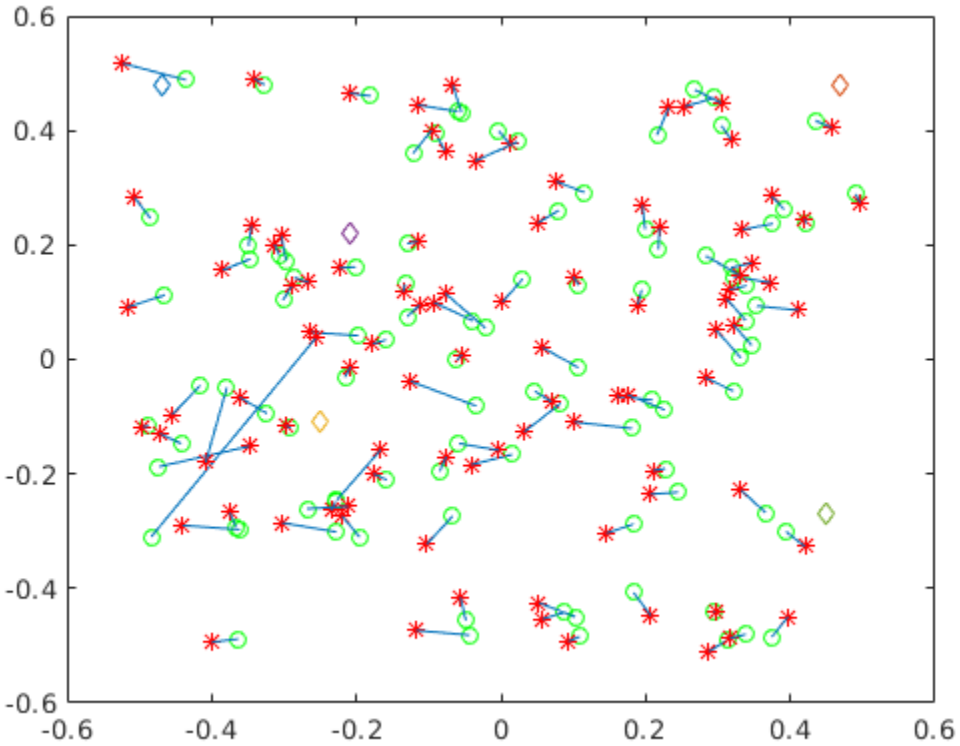

Figure 16 - Semidefinite Programming, transmission radius = 0.5 (Matlab)

At a transmission radius of 0.2 and a density of 100, average degree is 4.14 and results deteriorate, especially as distance from the anchors increases, as shown in Figure 17. These results show the need for a more robust strategy for localization when the WSN has small transmission radius relative to the field size and low degree of connectivity graph.

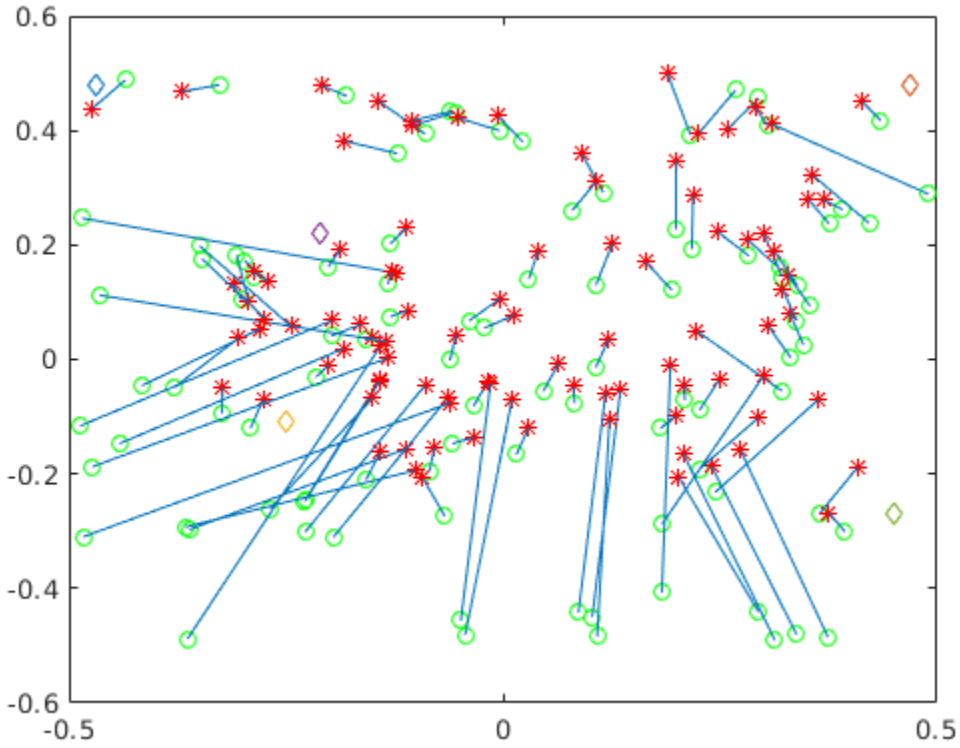

Figure 17 - Semidefinite Programming, transmission radius = 0.2 (Matlab)

4.3 Perpendicular Intersection

The UAV performs an equilateral triangulated traversal of the sensor field by making a turn as it reaches the vertex of each triangle as shown in Figure 18. Each node lies within one triangle of which two sides are traversed. Localization is computed for points within each triangle using only RSSI values found on these two sides. The localization is then refined as described above.

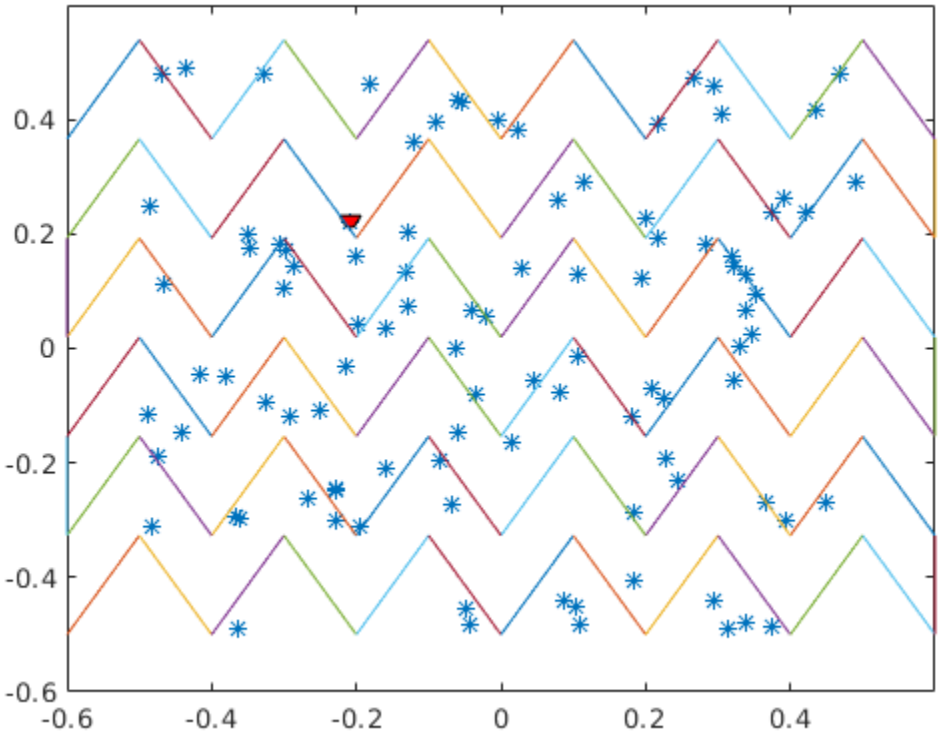

Figure 18 - Perpendicular Intersection Triangulation (Matlab)

4.4 Augmented Perpendicular Intersection – Equilateral Triangulation

The UAV performs an equilateral triangulated traversal of the sensor field by making turns only when an edge is encountered as shown in Figure 19. Localization is computed using all RSSI values received for a node, which may include more than two passes. RSSI traces will typically be longer than a triangle side. Multiple localizations may be tested.

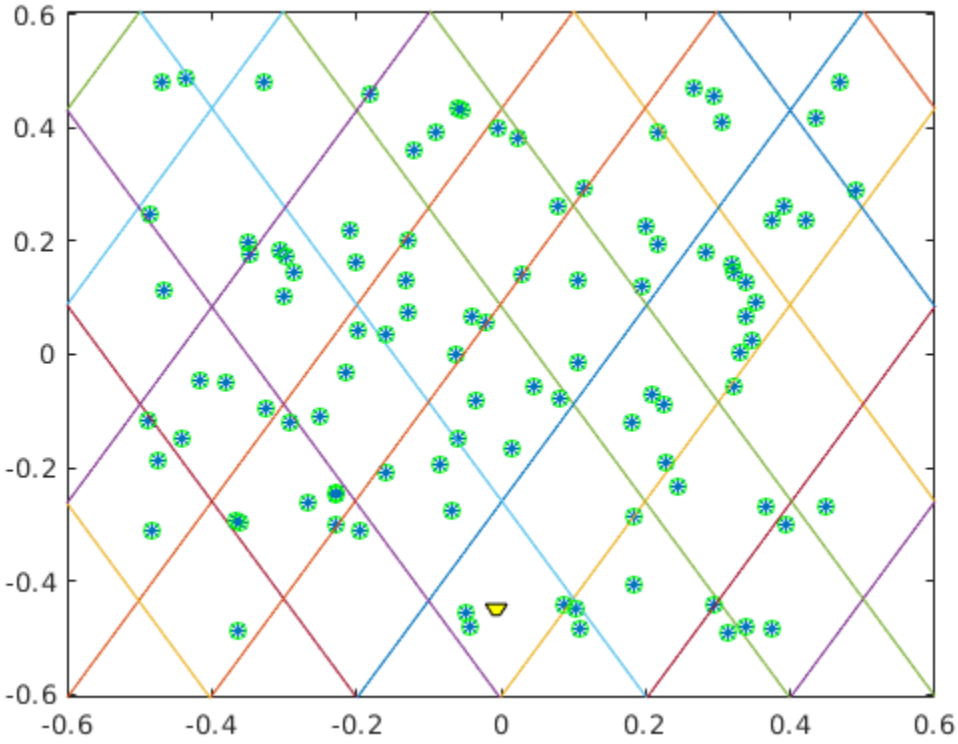

Figure 19 - Augmented PI: Equilateral Triangulation (Matlab)

4.5 Augmented Perpendicular Intersection – Isosceles Triangulation

The UAV performs an isosceles triangulated traversal of the sensor field by making turns only when an edge is encountered as shown in Figure 20. Acute angle is 0.166 rad. Less UAV travel and fewer turns are required compared to the equilateral triangulation. Multiple localizations may be tested.

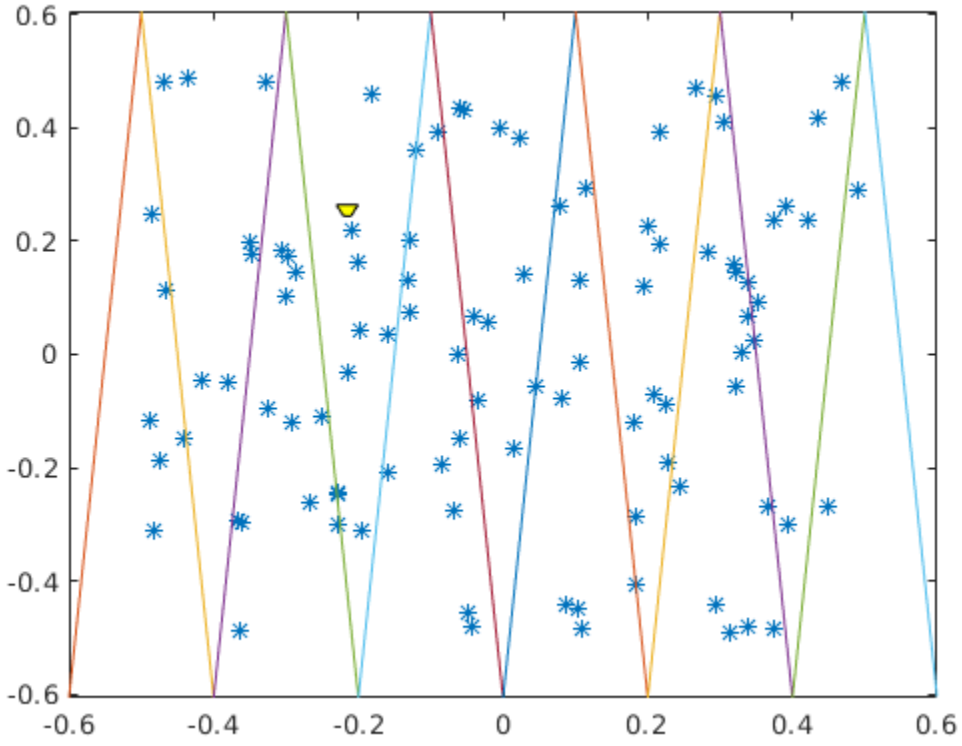

Figure 20 - Augmented PI: Isosceles Triangulation (Matlab)

Chapter 5: Results

Ten tests were run for each localization method. Field size is 100x100 metres, with 100 nodes following a two-dimension Poisson distribution. The initial scan is followed by an attempt to locate and charge each node. For other than original PI, the travel to the estimated location adds traces for other nodes. Transmission radius, abbreviated below as *u,* is 20 metres. The result fields are summarized below.

5.1 Description of Test Parameters and Results

5.1.1 Test parameters

Tests were run with charger EIRP of both 4W and 160W. The EIRP of 4W is the maximum for unlicensed use and gives a charging radius of about 1.8 metres at an altitude of 1.0 metre. The EIRP of 160W was chosen to give twice the charging radius, i.e. about 3.7 metres.

All tests were run with log normal fading of 4 dB at horizontal, adjusted for angle of attack.

5.1.2 Result Tables

Located by initial trajectory: The trajectory estimates were inside the charging footprint. Some tests used only one estimate, i.e. the "first" estimate using the longest up and down traces. Other tests used all estimates, subject to disk cover consolidation, and estimates farther than *u/2* from the "first" estimate being excluded, as they are likely outliers. Estimates are ordered based on distance from "first" estimate.

Located by refined PI: The trajectory estimates were outside the charging footprint. An extra equilateral triangulation is made to try to obtain a better estimate. This starts at side length *u/2* for equilateral PI and *u* for isosceles PI, with *u/2* then tried if the former fails.

Located by spiral: RSSI location is assumed to be ineffective and the UAV follows a spiral attempting to find the node within the charging radius.

Initial trajectory distance: the distance traveled by the initial tiling, in metres. The original PI has a smaller distance than the end-to-end tilings due to geometric requirements for the latter but requires many more turns.

Location trajectory distance: the distance traveled after the initial tiling as the UAV attempts to find the nodes, in metres.

Location error (histogram and CDF): the 100 error points, being the difference between the estimated location and the actual location, on the x axis in metres. Histogram count and cumulative distribution respectively on the y axis. For tests using all estimates, this is the error of the first estimated location that was found to be within the charging footprint.

5.1.3 Error Histograms

Figure 21, Figure 23, Figure 25, Figure 27, Figure 29. Figure 31, Figure 33, Figure 35, Figure 37, and Figure 39 are histograms of RSSI location error.

For tests with a single estimate (original PI, augmented PI limited to first estimate) this is the error of the single estimate. For tests with all estimates, this is the error of the first tested estimate which lies within the charging radius.

5.1.4 Error Empirical CDF

Figure 22, Figure 24, Figure 26, Figure 28, Figure 30, Figure 32,
Figure 34, Figure 36, Figure 38 and Figure 40 are cumulative distribution functions of the same data points as the previous error histograms. Each plot shows the minimum (min), maximum(max), mean, median, and standard deviation (std) of the error data.

5.2 Perpendicular Intersection (PI) original

This uses the original perpendicular intersection algorithm from [6] as described in 2.3. With charger EIRP of 4W the location by initial trajectory has a success rate of under 50%, i.e. 44.2%. However, accuracy is good enough for the added refined PI (traversing an additional triangle) to bring the combined success rate to 96.2%.

Equilateral tiling tested with 100 nodes and charger EIRP of 4W.

Test #	Located by initial trajectory	Located by refined PI	Located by spiral	Initial trajectory distance	Location trajectory distance	Total distance
1	42	55	3	1374.88	8503.10	9877.98
2	47	46	7	1374.88	8414.73	9789.61
3	41	53	6	1374.88	8806.31	10181.18
4	41	55	4	1374.88	8505.19	9880.06
5	43	52	5	1374.88	8557.28	9932.16
6	43	55	2	1374.88	8517.50	9892.38
7	47	52	1	1374.88	8443.80	9818.68
8	50	49	1	1374.88	8279.28	9654.16
9	46	48	6	1374.88	8456.93	9831.81
10	42	55	3	1374.88	8516.30	9891.18
AVG	44.2	52	3.8	1374.88	8500.04	9874.92

Table 1 - PI (original) EIRP = 4W

With charger EIRP of 160W the location by initial trajectory has a much higher success rate. This indicates that many of the location failures at 4W were just outside the charging footprint, which doubles when the power is increased to 160W After adding refined PI (traversing an additional triangle) the success rate is 99%. The location trajectory distance is decreased due to fewer refined PI attempts.

Equilateral tiling tested with 100 nodes and charger EIRP of 160W

Test #	Located by initial trajectory	Located by refined PI	Located by spiral	Initial trajectory distance	Location trajectory distance	Total distance
1	79	20	1	1374.88	8180.58	9555.46
2	80	19	1	1374.88	8007.56	9382.44
3	76	24	0	1374.88	8287.62	9662.50
4	82	15	3	1374.88	7792.86	9167.73
5	75	24	1	1374.88	8522.34	9897.21
6	84	15	1	1374.88	7879.69	9254.57
7	74	26	0	1374.88	8617.90	9992.77
8	72	25	3	1374.88	8540.63	9915.50
9	76	24	0	1374.88	8436.43	9811.30
10	82	18	0	1374.88	7863.91	9238.79
AVG	78	21	1	1374.88	8212.95	9587.83

Table 2 - PI (original) EIRP = 160W

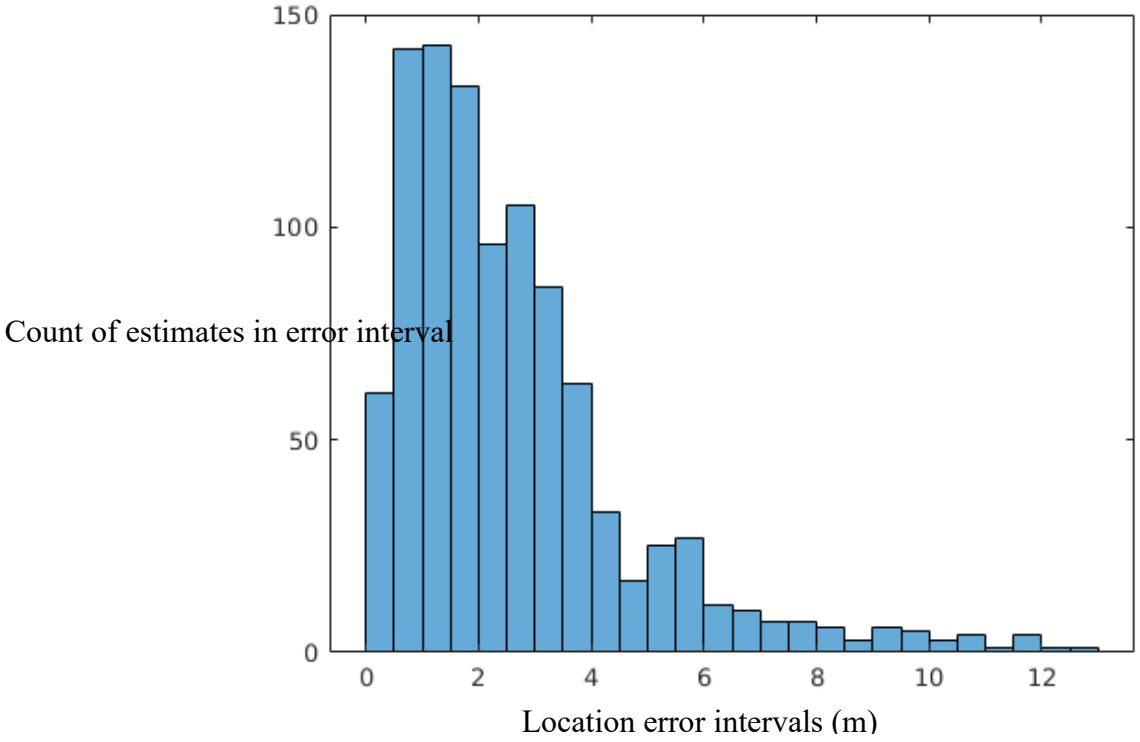

Figure 21 – PI (original) Histogram, EIRP=4W

From the histogram at Figure 21 it can be seen that the most likely location ranges are found from 0.5m to 2.0m. Given the charging footprint radius is 1.7m at 4W EIRP this shows that there are many "near misses" among the original trajectory estimates.

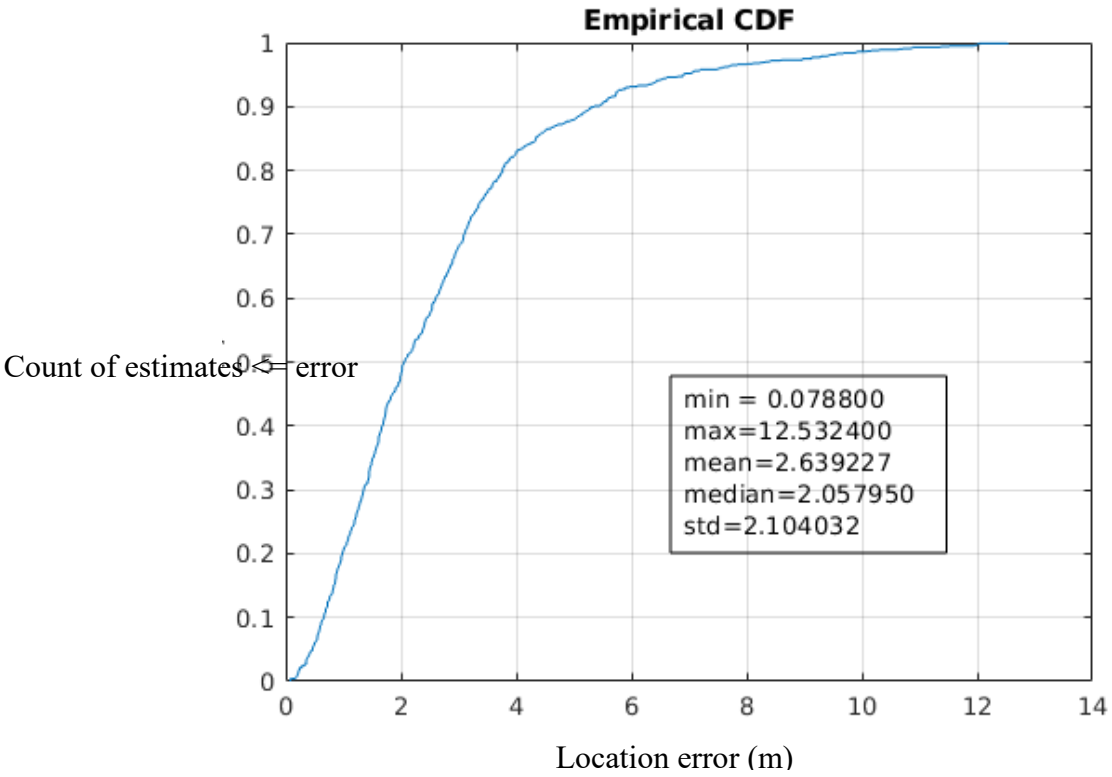

Figure 22 – PI (original) CDF, EIRP=4W

The cumulative distribution of location error increases almost linearly up to 2.0, and then almost linearly with a smaller slope up to 4.0, then tapers off.

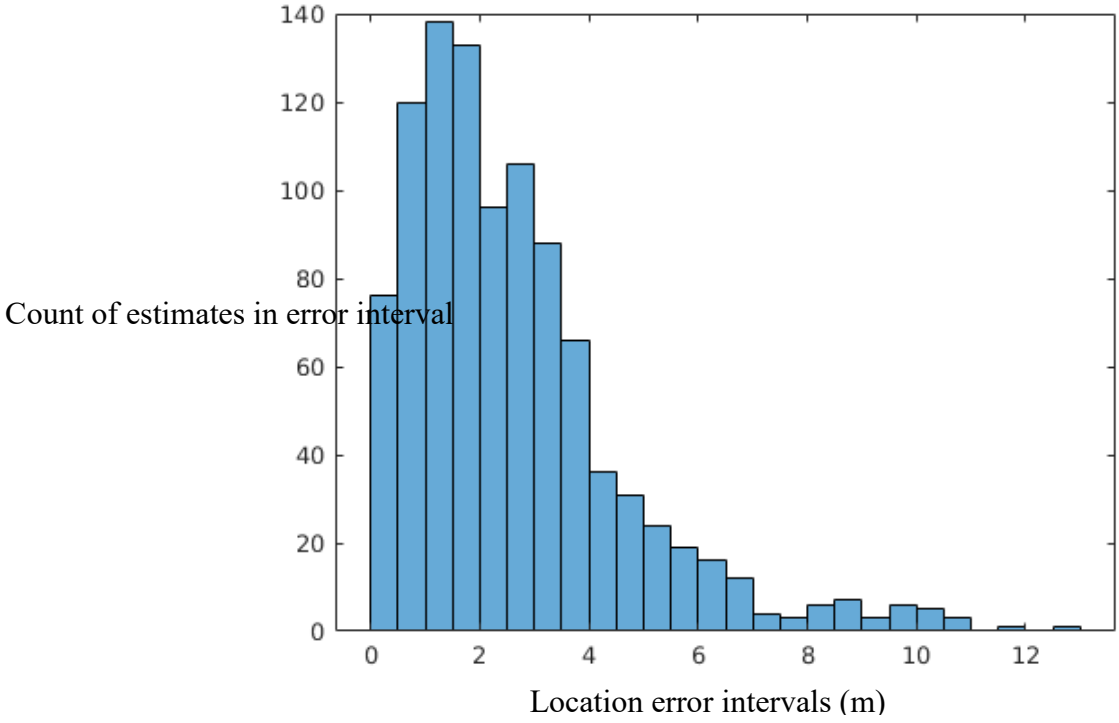

Figure 23 - PI (original) Histogram, EIRP=160W

Subject to randomness of the test, this histogram is very similar to Figure 21 – PI (original) Histogram, EIRP=4W. This is to be expected as only one estimate is generated for each node, thus the error is independent of the charger EIRP.

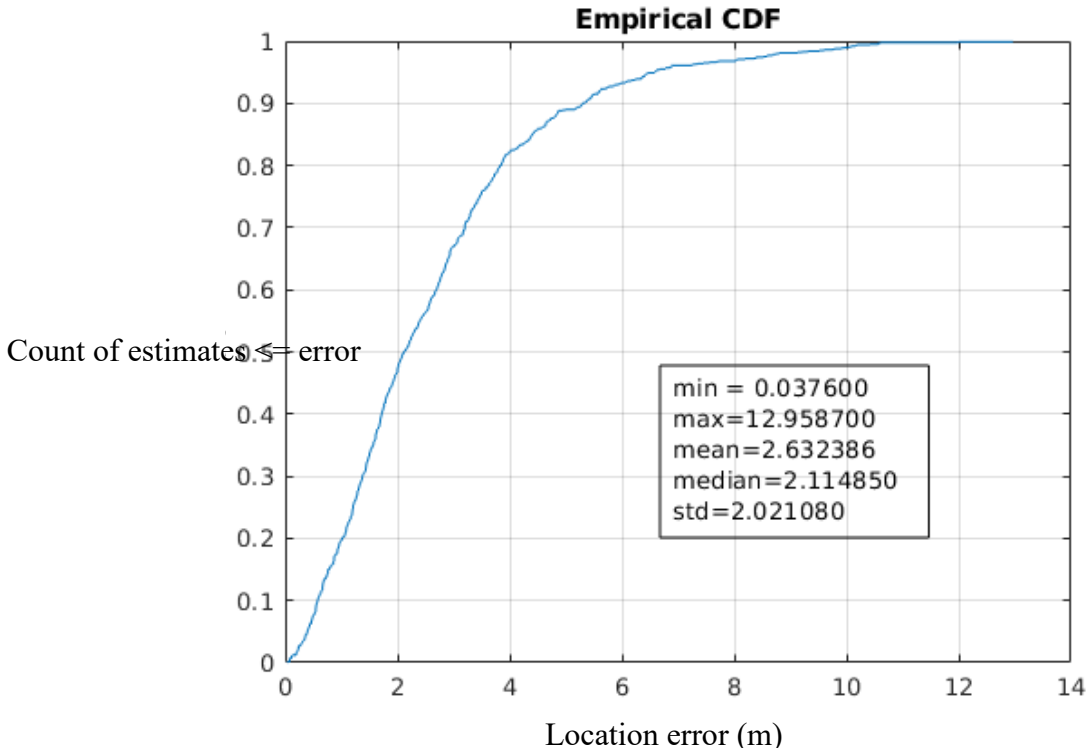

Figure 24 - PI (original) CDF, EIRP=160W

Subject to randomness of the test, this CDF is very similar to Figure 22 – PI (original) CDF, EIRP=4W. This is to be expected as only one estimate is generated for each node, thus the error is independent of the charger EIRP.

5.3 Augmented PI, Equilateral Tiling, Test First Intersection Only

Augmented PI usually produces multiple intersection estimates, but only the first ranked is tested here, i.e. from the intersection of the longest up and down traces.

Compared to the original PI, the augmented PI using first estimate increases success of initial trajectory from 44.2% to 48.1%. This is due to the more complete RSSI collection by the initial trajectory (as described in paragraph 3.2).

End to end equilateral tiling with 100 nodes and charger EIRP of 4 W.

Test #	Located by initial trajectory	Located by refined PI	Located by spiral	Initial trajectory distance	Location trajectory distance	Total distance
1	58	40	2	1694.17	8152.40	9846.56
2	43	52	5	1694.23	8596.27	10290.50
3	44	51	5	1694.17	8574.11	10268.28
4	51	41	8	1694.23	8464.84	10159.07
5	49	45	6	1694.22	8457.88	10152.10
6	50	46	4	1694.17	8459.72	10153.89
7	43	53	4	1694.28	8683.87	10378.15
8	48	47	5	1694.47	8487.03	10181.51
9	49	47	4	1694.23	8479.35	10173.57
10	46	49	5	1694.28	8692.49	10386.77
AVG	48.1	47.1	4.8	1694.24	8504.80	10199.04

Table 3 - Augmented PI, Equilateral, First Intersection, EIRP = 4W

With charger EIRP of 160W, no significant difference from original PI is observed. This is because doubling of the radius of the charging footprint is much more significant than the improvement in localization accuracy.

End to end equilateral tiling with 100 nodes and charger EIRP of 160W.

Test #	Located by initial trajectory	Located by refined PI	Located by spiral	Initial trajectory distance	Location trajectory distance	Total distance
1	78	21	1	1694.17	9475.39	11169.56
2	80	20	0	1694.35	9577.61	11271.96
3	81	19	0	1694.17	9339.30	11033.47
4	80	18	2	1694.17	9429.71	11123.88
5	81	18	1	1694.17	9617.40	11311.57
6	77	23	0	1694.38	9657.82	11352.21
7	78	22	0	1694.17	9588.87	11283.04
8	80	20	0	1694.35	9577.61	11271.96
9	81	19	0	1694.17	9339.30	11033.47
10	80	18	2	1694.17	9429.71	11123.88
AVG	79.6	19.8	0.6	1694.23	9503.27	11197.50

Table 4 - Augmented PI, Equilateral, First Intersection, EIRP = 160W

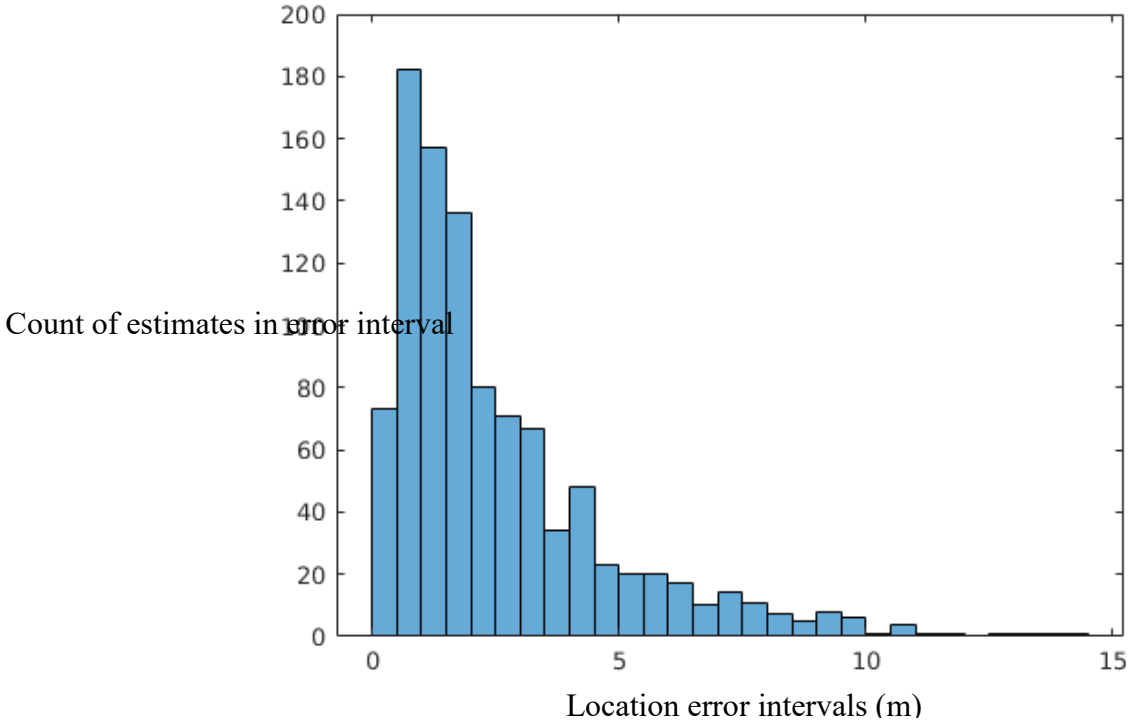

Figure 25 - Augmented PI, Equilateral, First Intersection Histogram, EIRP=4W

Compared to Figure 21 – PI (original) Histogram, EIRP=4W, there is a shift of the peak to a lower error interval, indicating increased accuracy as discussed above.

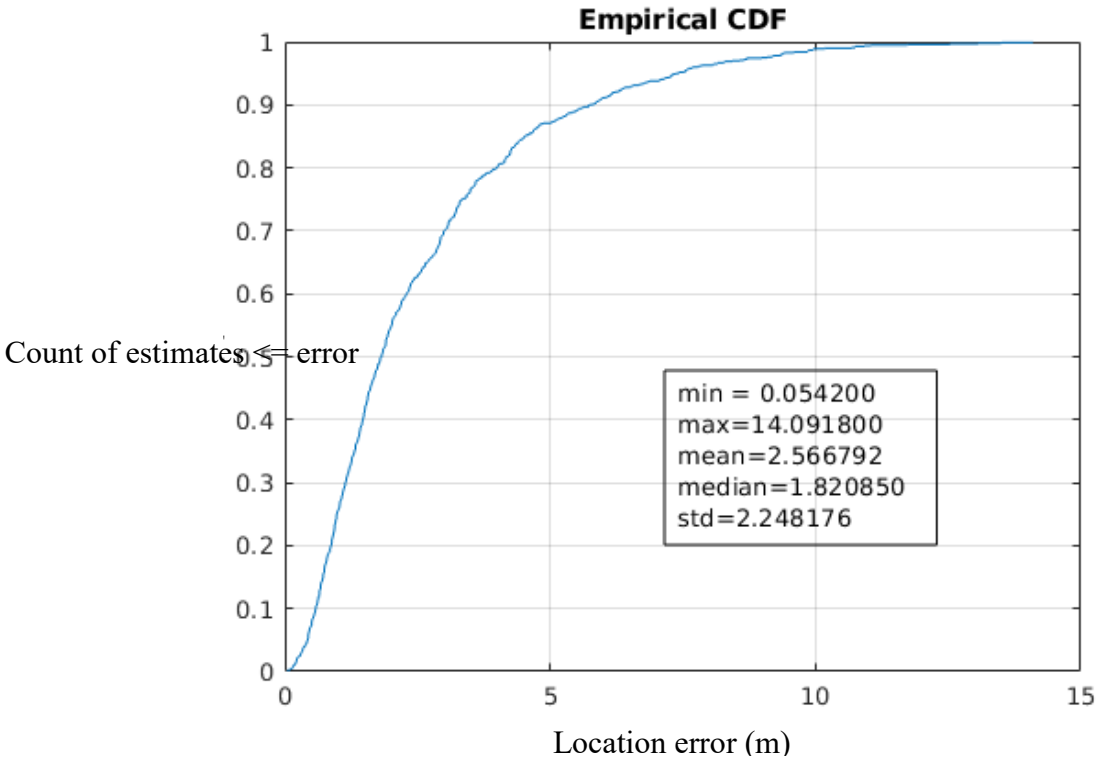

Figure 26 - Augmented PI, Equilateral, First Intersection CDF, EIRP=4W

Compared to Figure 22 – PI (original) CDF, EIRP=4W, a decrease in mean and median error can be seen, indicating increased accuracy as discussed above.

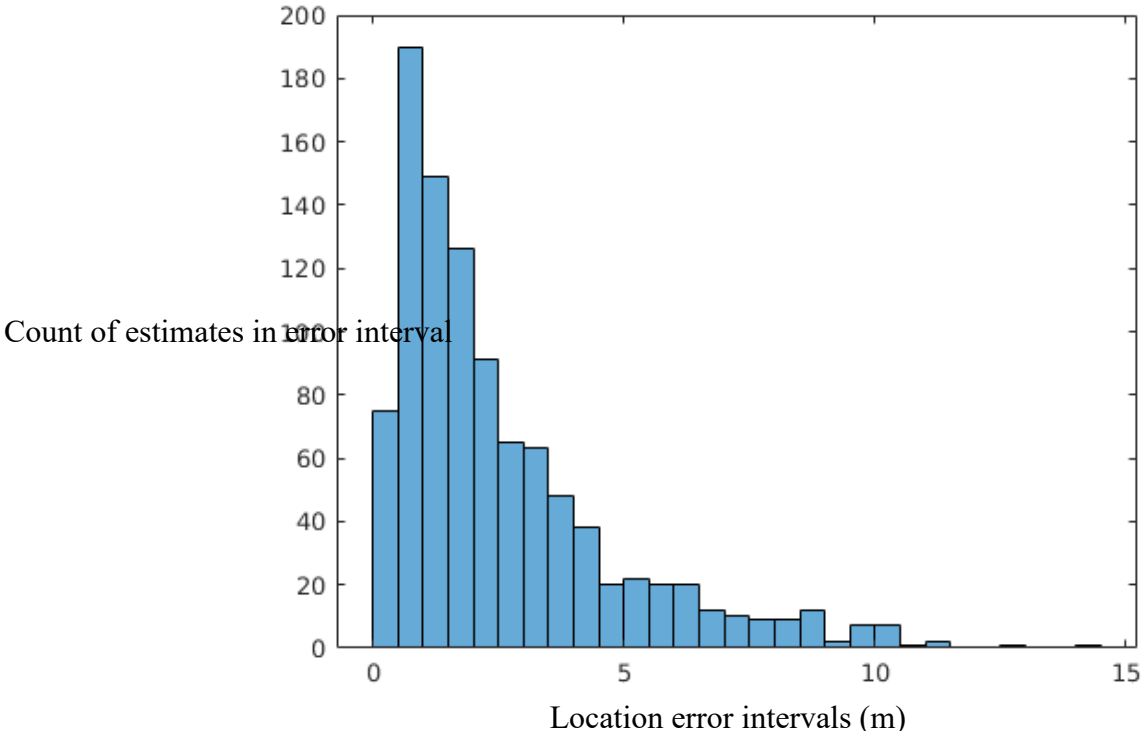

Figure 27 - Augmented PI, Equilateral, First Intersection Histogram, EIRP=160W

Subject to randomness of the test, this histogram is very similar to Figure 25 - Augmented PI, Equilateral, First Intersection Histogram, EIRP=4W. This is to be expected as only one estimate is tested for each node, thus the error is independent of the charger EIRP.

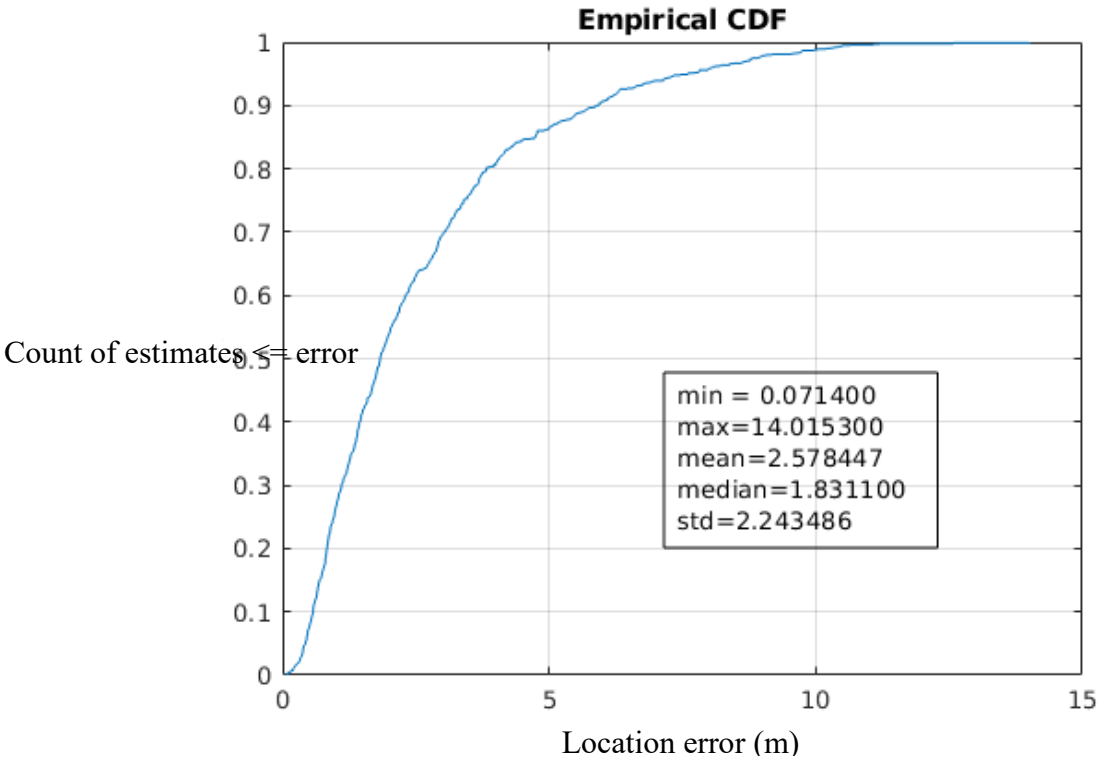

Figure 28 - Augmented PI, Equilateral, First Intersection CDF, EIRP=160W

Subject to randomness of the test, this CDF is very similar to Figure 26 - Augmented PI, Equilateral, First Intersection CDF, EIRP=4W. This is to be expected as only one estimate is tested for each node, thus the error is independent of the charger EIRP.

5.4 Augmented PI, Equilateral Tiling, Test All Intersections

All intersections tested until in charging footprint, subject to disk cover consolidation.

End to end equilateral tiling with 100 nodes and charger EIRP of 4 W.

Compared to augmented PI using first estimate, the augmented PI using all estimates increases success of initial trajectory from 48.1% to 71.8%. This shows the increased accuracy of the strategy of calculating and testing multiple estimates using all available RSSI data.

The location trajectory distance can be seen to decrease from 8505 m to 8127 m, showing the success of the multiple estimates in reducing UAV travel.

Test #	Located by initial trajectory	Located by refined PI	Located by spiral	Initial trajectory distance	Location trajectory distance	Total distance
1	73	22	5	1694.37	8153.22	9847.59
2	71	26	3	1694.17	8160.35	9854.52
3	70	28	2	1694.47	8172.94	9867.41
4	73	25	2	1694.24	8119.93	9814.18
5	74	22	4	1694.40	7879.73	9574.14
6	73	25	2	1694.17	8187.11	9881.28
7	75	22	3	1694.17	7994.82	9688.99
8	69	28	3	1694.39	8285.26	9979.65
9	69	25	6	1694.23	8138.36	9832.59
10	71	23	6	1694.17	8178.89	9873.06
AVG	71.8	24.6	3.6	1694.28	8127.06	9821.34

Table 5 - Augmented PI, All Intersections, EIRP = 4W

End to end equilateral tiling with 100 nodes and charger EIRP of 160 W.

With charger EIRP of 160W, the success rate of initial trajectory increases from 71.8% to 88.9% due to the doubling of the radius of the charging footprint. However, the location trajectory distance increases from 8127 m to 9268 m despite this. This is because the testing of estimates stops with the first estimate within the charging footprint, and this may mean a better estimate is missed. The UAV then traverses a greater distance within the charging footprint during ToC refinement.

Test #	Located by initial trajectory	Located by refined PI	Located by spiral	Initial trajectory distance	Location trajectory distance	Total distance
1	87	12	1	1694.23	9230.77	10924.99
2	88	10	2	1694.22	9387.60	11081.82
3	89	10	1	1694.22	9380.01	11074.23
4	86	12	2	1694.35	9308.61	11002.96
5	92	8	0	1694.22	9241.98	10936.19
6	88	12	0	1694.34	9231.05	10925.39
7	90	9	1	1694.22	9246.37	10940.59
8	88	12	0	1694.17	9191.62	10885.79
9	90	10	0	1694.17	9091.98	10786.15
10	91	9	0	1694.22	9368.84	11063.06
AVG	88.9	10.4	0.7	1694.24	9267.88	10962.12

Table 6 - Augmented PI, All Intersections, EIRP = 160W

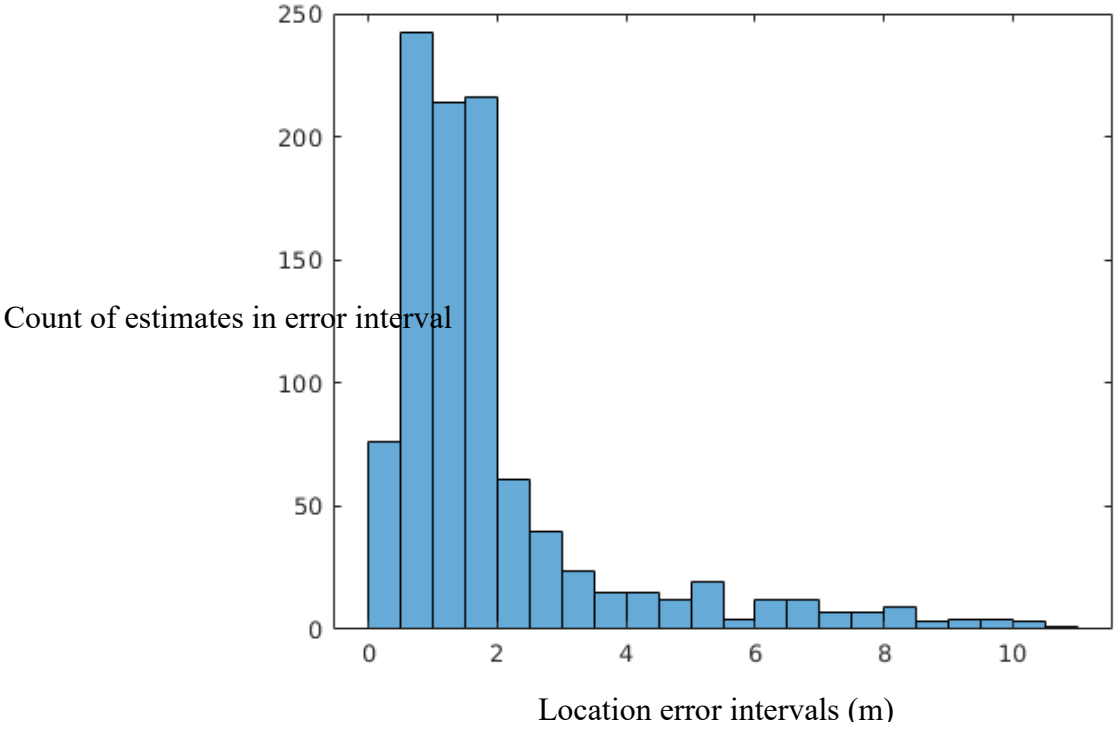

Figure 29 - Augmented PI, Equilateral, All Intersections Histogram, EIRP=4W

The increased number of estimates with error <= 2 m is apparent in comparison to Figure 25 - Augmented PI, Equilateral, First Intersection Histogram, EIRP=4W.

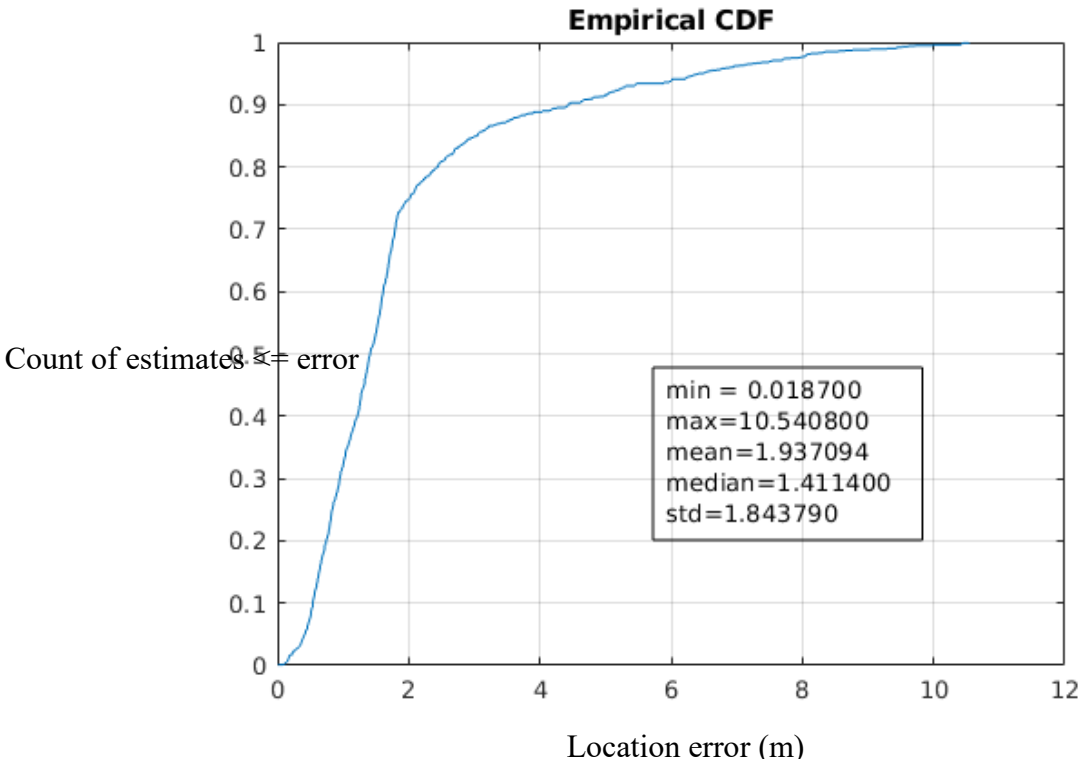

Figure 30 - Augmented PI, Equilateral, All Intersections CDF, EIRP=4W

Compared to Figure 26 - Augmented PI, Equilateral, First Intersection CDF, EIRP=4W, the mean error is seen to decrease from 2.56 m to 1.94 m, and the median error from 1.82 m to 1.41 m.

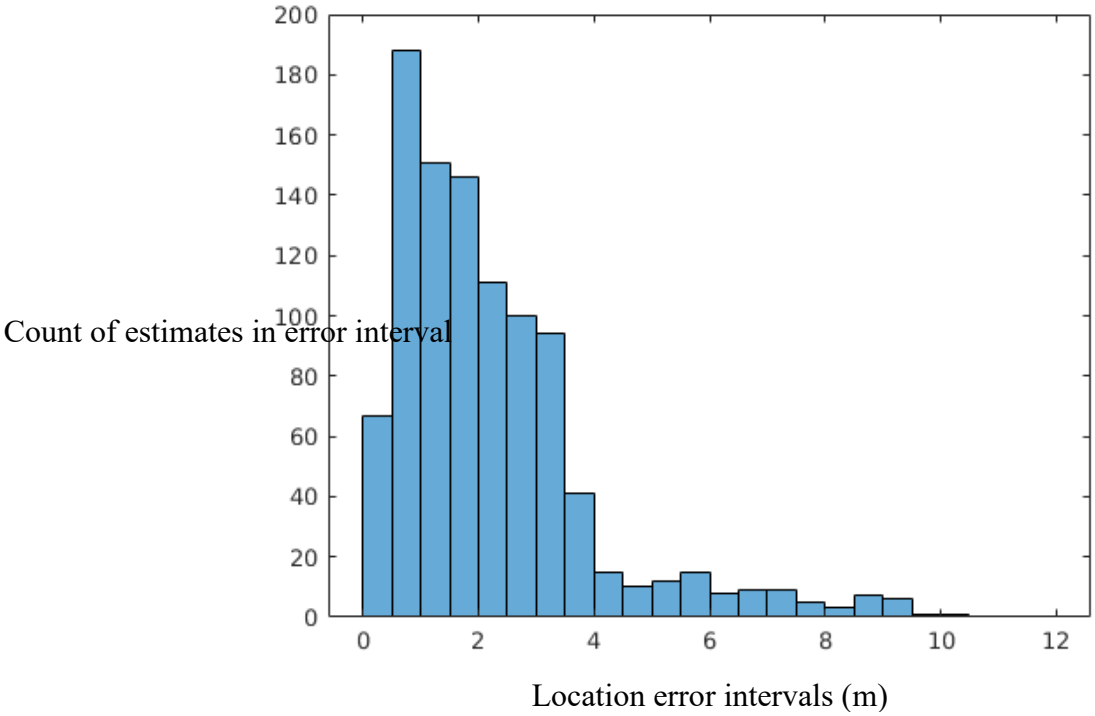

Figure 31 - Augmented PI, Equilateral, All Intersections Histogram, EIRP=160W

As discussed above, more estimates are logged with error > 2 m due to the doubling of the radius of the charging footprint.

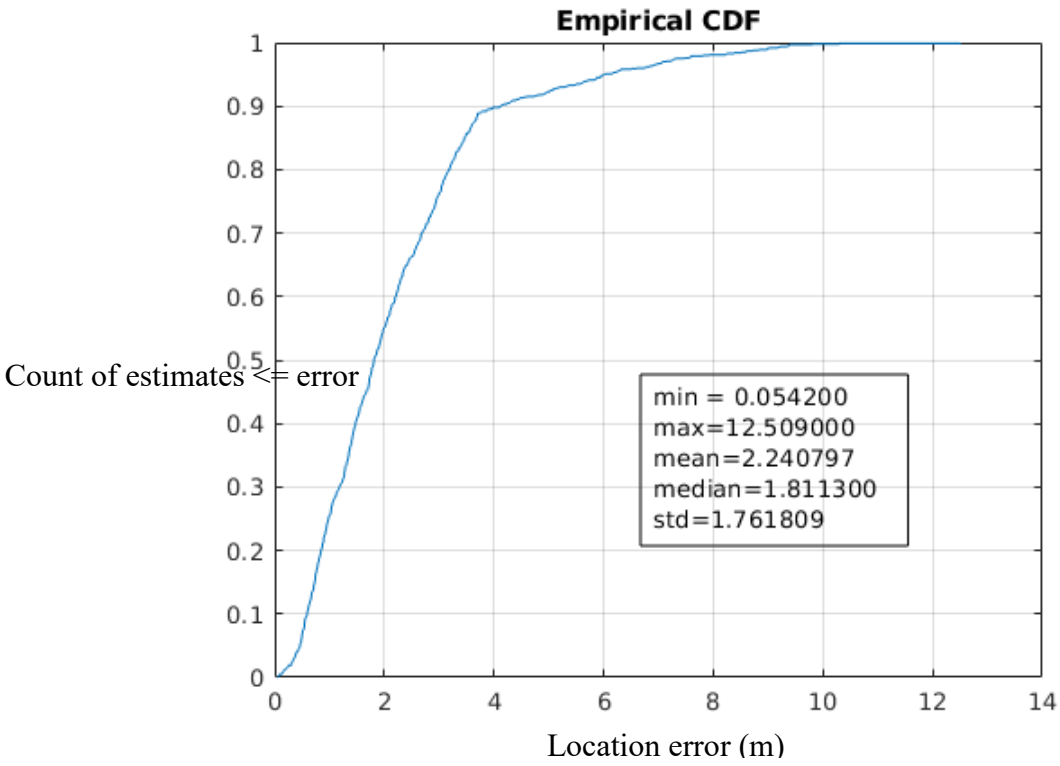

Figure 32 - Augmented PI, Equilateral, All Intersections CDF, EIRP=160W

Compared to Figure 30 - Augmented PI, Equilateral, All Intersections CDF, EIRP=4W, the mean error increases from to 1.91 to 2.24 m, and the median error increases from 1.41 m to 1.81 m.

5.5 Augmented PI, Isosceles Tiling, Test First Intersection Only

End to end isosceles tiling with 100 nodes and charger EIRP of 4 W.

This trajectory shows a large deterioration in localization accuracy compared to all the equilateral trajectory options. Total distance increases greatly despite the reduced initial trajectory distance. The acute angle of the trajectories results in an oblique angle of the perpendiculars. This magnifies the effect of any error in locating the base of the perpendiculars based on received RSSI. The mean distance from MAN to node is also larger increasing fading.

Test #	Located by initial trajectory	Located by refined PI	Located by spiral	Initial trajectory distance	Location trajectory distance	Total distance
1	16	63	21	1474.05	23673.07	25147.12
2	17	65	18	1474.05	19238.05	20712.10
3	23	66	11	1473.95	16875.06	18349.01
4	17	70	13	1473.95	17419.42	18893.38
5	11	81	8	1473.95	16361.32	17835.27
6	10	74	16	1473.95	21128.13	22602.08
7	19	66	15	1474.05	20818.08	22292.13
8	15	73	12	1474.05	16878.60	18352.65
9	26	66	8	1473.95	17558.41	19032.37
10	20	64	16	1473.95	19537.98	21011.93
AVG	17.4	68.8	13.8	1473.99	18948.81	20422.80

End to end isosceles tiling with 100 nodes and charger EIRP of 160 W.

The doubling of the charging footprint from the higher power almost doubles the success rate from the initial trajectory, but the rate is still under 1 in 3 and the total distance is still very high.

Test #	Located by initial trajectory	Located by refined PI	Located by spiral	Initial trajectory distance	Location trajectory distance	Total distance
1	29	62	9	1473.95	17034.46	18508.42
2	40	51	9	1473.95	15985.38	17459.33
3	32	58	10	1473.95	17201.79	18675.74
4	37	54	9	1473.95	16022.45	17496.40
5	36	56	8	1473.95	16327.75	17801.71
6	30	64	6	1473.95	15252.12	16726.07
7	26	66	8	1473.95	17541.13	19015.08
8	36	54	10	1473.95	18105.27	19579.22
9	28	63	9	1473.95	15883.31	17357.27
10	30	65	5	1473.95	16530.50	18004.45
AVG	32.4	59.3	8.3	1473.95	16588.42	18062.37

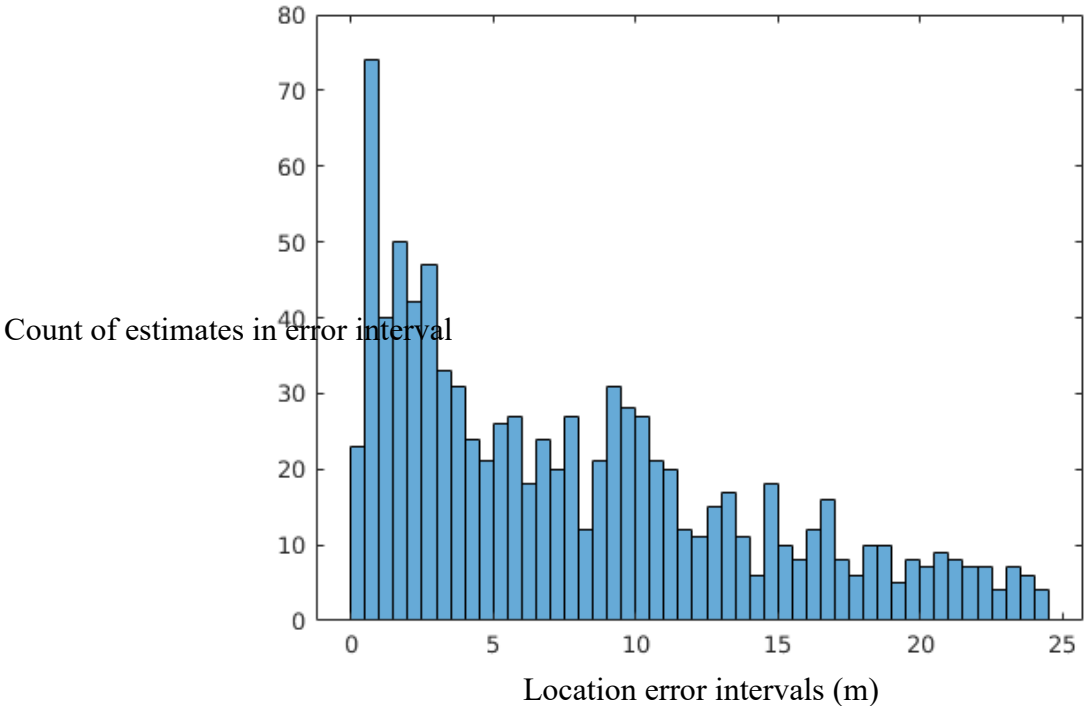

Figure 33 - Augmented PI, Isosceles, First Intersection Histogram, EIRP=4W

The histogram shows a very high number of errors beyond 2 m and a significant number of errors beyond the transmission radius of 20 m, which means an attempt at refined PI will likely fail due to being out of range.

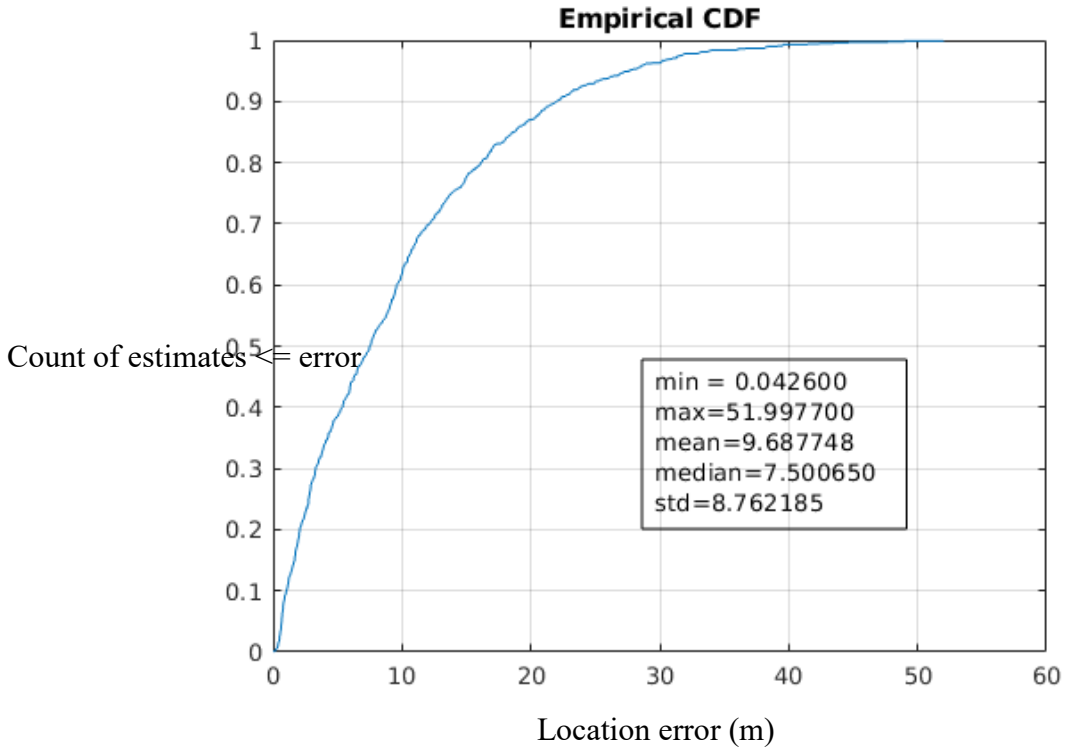

Figure 34 – Augmented PI, Isosceles, First Intersection CDF, EIRP=4W

The slow decline in the slope of the curve indicates significant numbers of estimates with large errors.

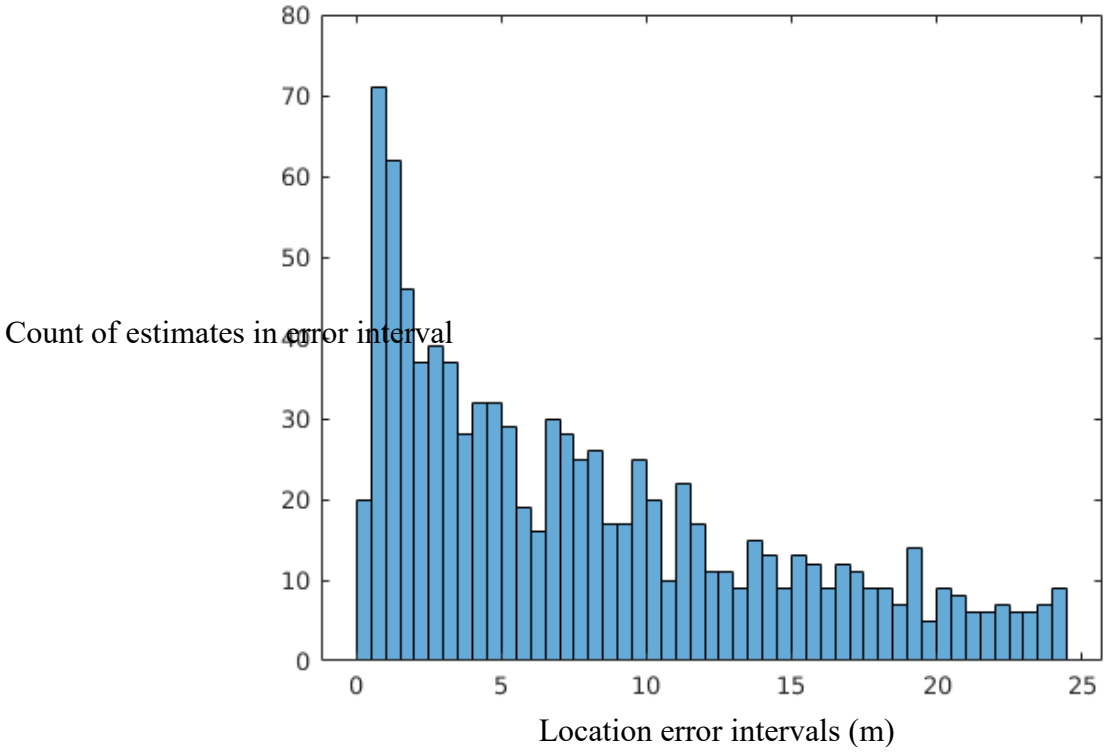

Figure 35 - Augmented PI, Isosceles, First Intersection Histogram, EIRP=160W

Not significantly different from Figure 33 - Augmented PI, Isosceles, First Intersection Histogram, EIRP=4W since first estimate error does not depend on charging power.

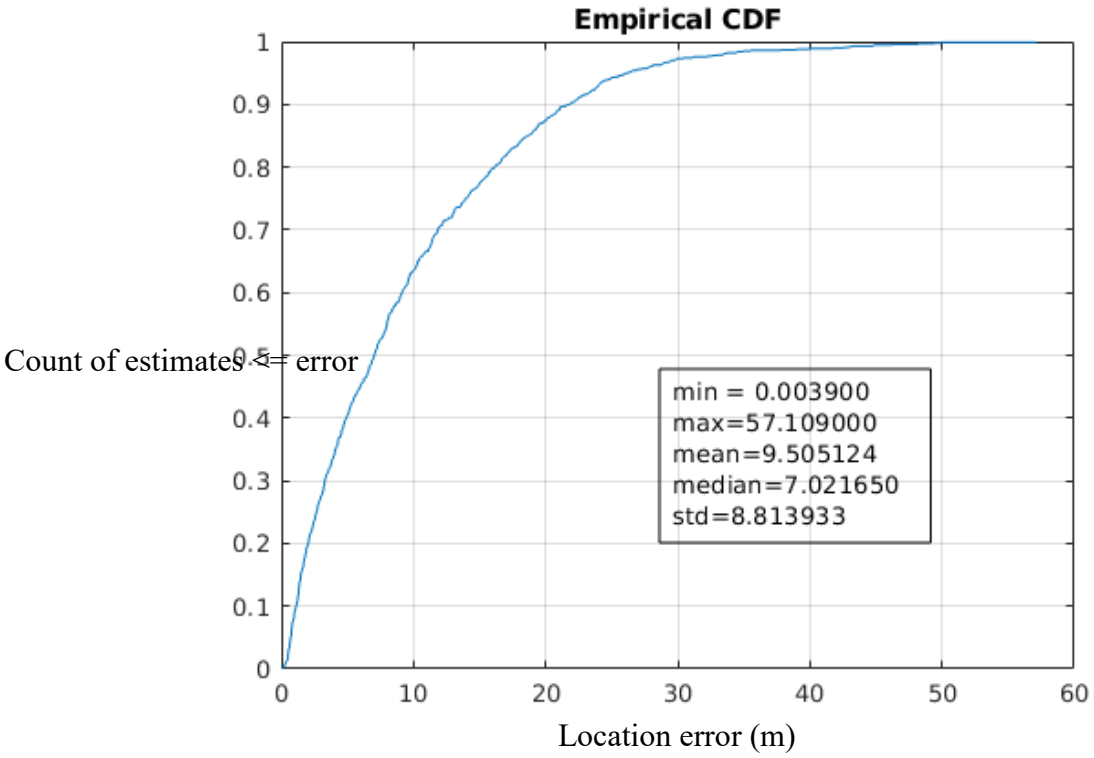

Figure 36 - Augmented PI, Isosceles, First Intersection CDF, EIRP=160W

Not significantly different from Figure 34 – Augmented PI, Isosceles, First Intersection CDF, EIRP=4W since first estimate error does not depend on charging power.

5.6 Augmented PI, Isosceles Tiling, Test All Intersections

All intersections tested until in charging footprint, subject to disk cover consolidation.

End to end isosceles tiling with 100 nodes and charger EIRP of 4.

The success rate of location by initial trajectory doubles from first intersection only to 35.3%. The testing of all intersections increases the probability of an accurate estimate being tested. Accuracy remains below all triangular trajectories and total distance remains higher.

Test #	Located by initial trajectory	Located by refined PI	Located by spiral	Initial trajectory distance	Location trajectory distance	Total distance
1	46	44	10	1474.05	14060.90	15534.95
2	28	55	17	1473.95	19557.75	21031.70
3	38	47	15	1474.05	17266.76	18740.81
4	26	58	16	1474.05	22184.85	23658.90
5	40	48	12	1473.95	17220.16	18694.12
6	36	55	9	1473.95	15195.66	16669.61
7	26	62	12	1473.95	20221.00	21694.96
8	40	53	7	1474.05	14485.91	15959.97
9	39	49	12	1473.95	15411.24	16885.19
10	34	56	10	1473.95	16155.18	17629.14
AVG	35.3	52.7	12	1473.99	17175.94	18649.93

End to end isosceles tiling with 100 nodes and charger EIRP of 160.

The success rate of location by initial trajectory improves to 49.4% which is better than for original PI, but the total distance remains greater than for all triangular trajectories.

Test #	Located by initial trajectory	Located by refined PI	Located by spiral	Initial trajectory distance	Location trajectory distance	Total distance
1	52	41	7	1474.05	14651.77	16125.82
2	46	47	7	1473.95	16673.12	18147.07
3	52	39	9	1474.05	15375.75	16849.80
4	45	43	12	1474.05	16519.65	17993.70
5	48	47	5	1474.05	14212.12	15686.17
6	53	42	5	1474.05	13567.92	15041.97
7	50	41	9	1474.05	15883.59	17357.64
8	50	37	13	1473.95	16950.15	18424.11
9	48	47	5	1473.95	15350.21	16824.16
10	50	38	12	1473.95	16541.20	18015.16
AVG	49.4	42.2	8.4	1474.01	15572.55	17046.56

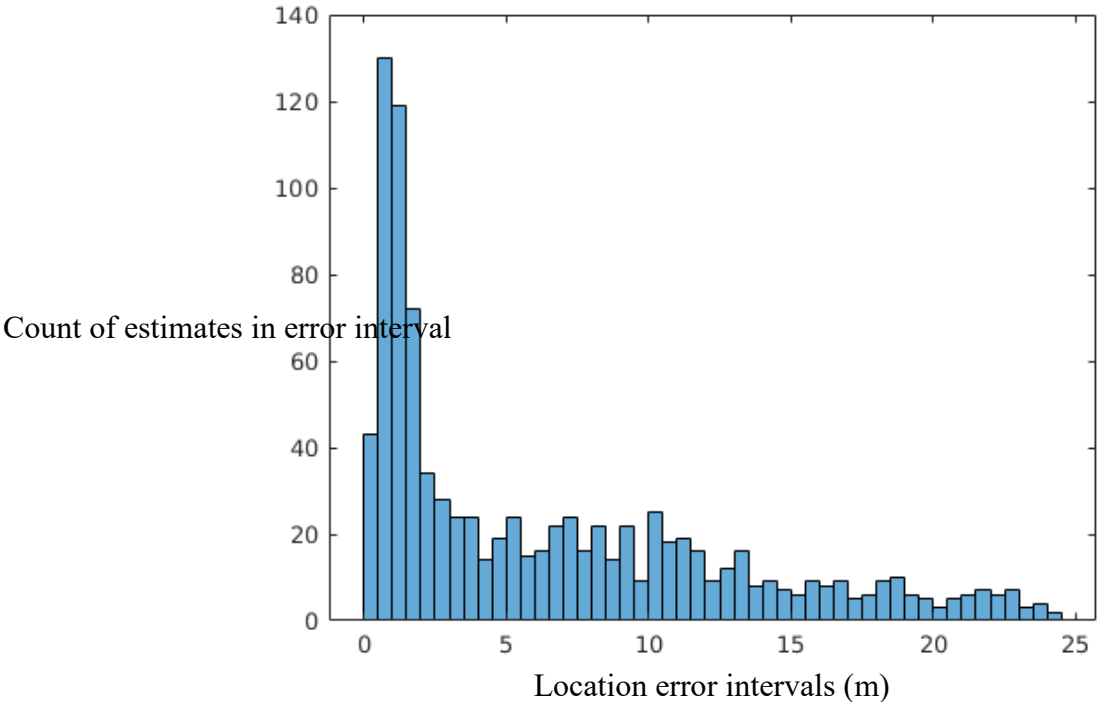

Figure 37 - Augmented PI, Isosceles, All Intersections Histogram, EIRP=4W

There is a substantial increase in the number of estimates in the error range > 0.5 and < 2.0 compared to Figure 33 - Augmented PI, Isosceles, First Intersection Histogram, EIRP=4W achieved by testing all intersections.

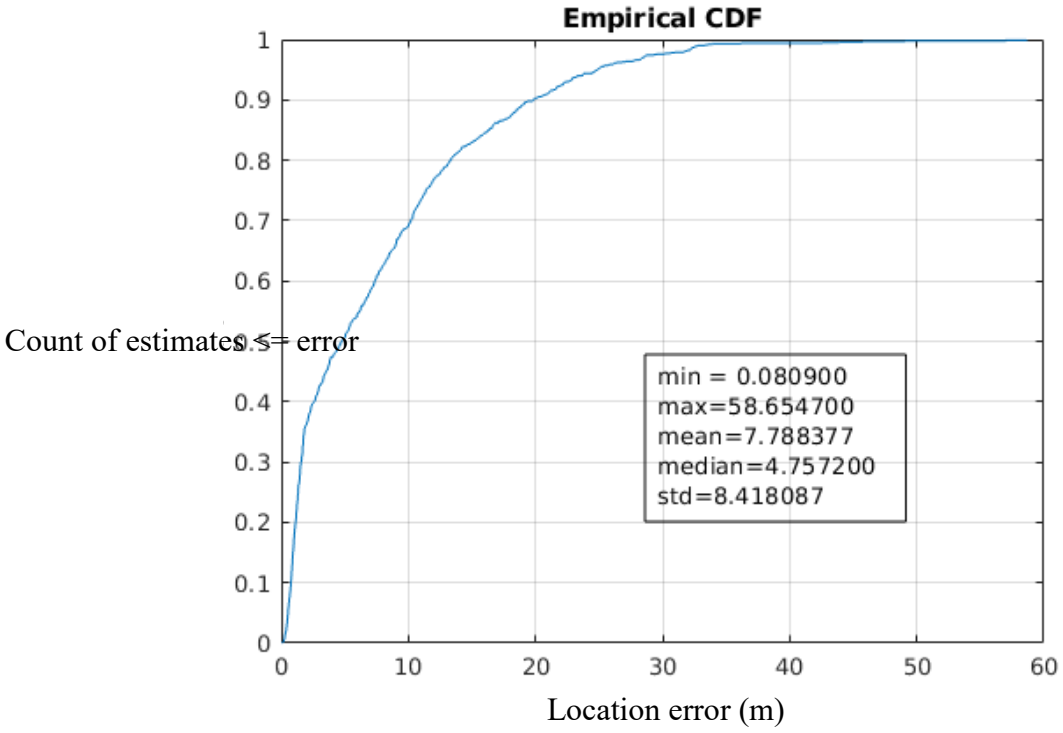

Figure 38 - Augmented PI, Isosceles, All Intersections CDF, EIRP=4W

The higher initial slope compared to Figure 34 – Augmented PI, Isosceles, First Intersection CDF, EIRP=4W reflects the larger number of estimates tested.

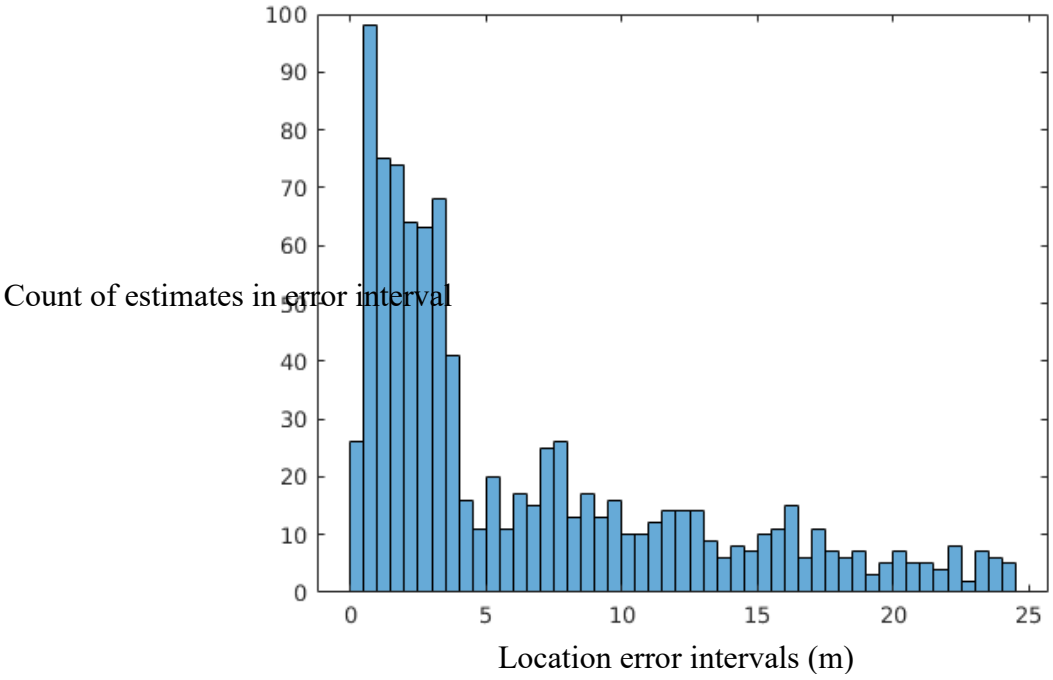

Figure 39 - Augmented PI, Isosceles, All Intersections Histogram, EIRP=160W

The increase in charging footprint radius from 1.7 m to 3.5 m results in estimates in this error range ending the estimate testing. This means the histogram shows more errors in this range and fewer in higher ranges compared to Figure 37 - Augmented PI, Isosceles, All Intersections Histogram, EIRP=4W.

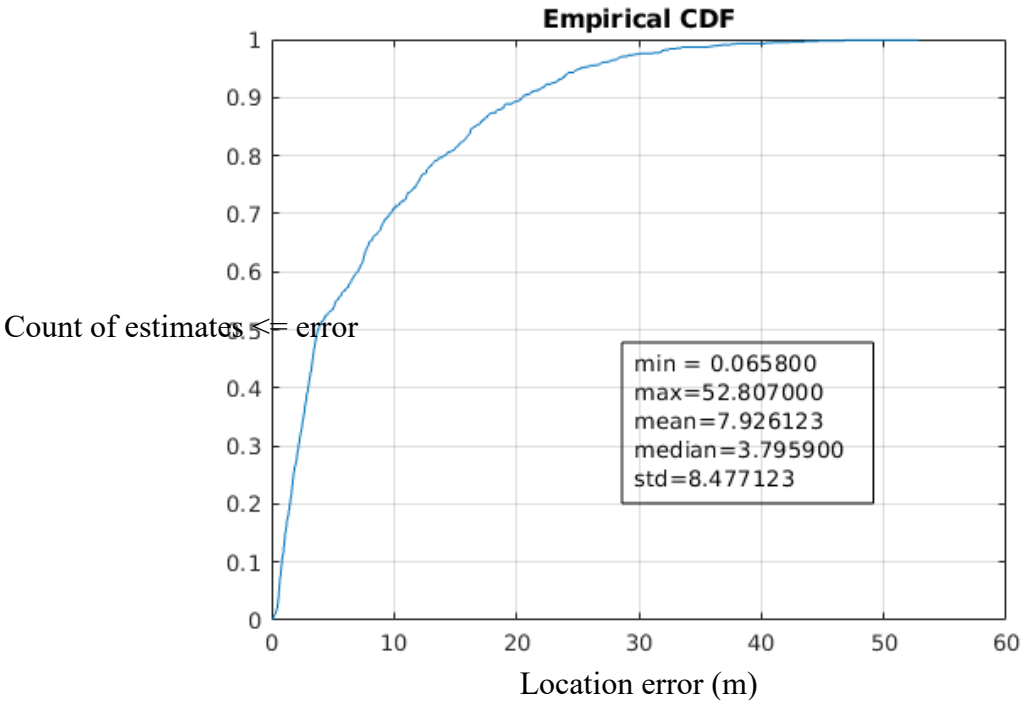

Figure 40 - Augmented PI, Isosceles, All Intersections CDF, EIRP=160W

Larger mean error 7.92 m versus 7.78 m but smaller median error 3.80 m versus 4.76 m compared to Figure 38 - Augmented PI, Isosceles, All Intersections CDF, EIRP=4W.

Chapter 6: Conclusions

6.1 Initial scan

The initial scan parameters are summarized below:

Type	***RSSI Scan Length***	***Trajectory Distance (m)***	***Number of Turns***
PI (original)	Fixed, *u*	1375	78 (at each vertex)
Augmented PI equilateral	Variable, at least *u*	1694	17 (at all 4 edges)
Augmented PI isosceles	Variable, at least *u*	1474	11 (at upper, lower edges)

It can be seen that the original PI has the smallest trajectory distance, however at the expense of a great number of turns. Augmented PI isosceles has a slightly larger distance and the smallest number of turns. Augmented PI equilateral has the largest distance and about 50% more turns than isosceles. In actual implementation there will be a tradeoff between distance and number of turns as the latter take time and energy.

6.2 Localization Error Statistics

Type	*min (m)*	*max (m)*	*mean (m)*	*median (m)*	*standard deviation (m)*
PI (original) 4W	0.079	12.53	2.64	2.058	2.10
PI (original) 160W	0.038	12.96	2.63	2.11	2.02
Augmented PI equilateral first intersection 4W	0.054	14.09	2.57	1.82	2.25
Augmented PI equilateral first intersection 160W	0.071	14.02	2.58	1.83	2.24
Augmented PI equilateral all intersections 4W	0.019	10.54	1.94	1.41	1.84
Augmented PI equilateral all intersections 160W	0.054	12.51	2.24	1.81	1.76
Augmented PI isosceles first intersection 4W	0.043	52.00	9.69	7.50	8.76
Augmented PI isosceles first intersection 160W	0.0039	57.11	9.50	7.02	8.81
Augmented PI isosceles all intersections 4W	0.081	58.65	7.79	4.75	8.42
Augmented PI isosceles all intersections 160W	0.066	52.81	7.93	3.80	8.48

There is no significant difference in the error statistics between PI (original) 4W and 160W. This is because there is only one intersection to be compared against the actual

location. Likewise, the first intersection tests for Augmented PI for equilateral and isosceles do not yield a significant difference between 4W and 160W.

However, for Augmented PI equilateral testing all intersections, the higher power results in a higher mean and median error. This is because intersections are tested until one is found within the charging footprint and this determines the localization error. With a higher power, a less accurate intersection is likely to be found first.

Testing all intersections produces a significant reduction in error for all modes for a given charger EIRP. The more traces that are used, the more likely a pair will be used that defines an accurate location estimate.

The equilateral triangulations all yield a maximum error less than u, which means that when the estimated location is not within the charging footprint a refinement triangulation is likely to be effective. The isosceles triangulations all have a much larger maximum error, and about 10% of intersections are more than u from the actual location, which means a refinement triangulation will not be effective in these cases.

6.3 Confidence Levels for Localization

Type	*Locatable by initial trajectory (%)*	*Locatable by refined PI (%)*	*Locatable by spiral (%)*
PI (original) 4W	44.2	96.2	100
PI (original) 160W	78	94.6	100
Augmented PI equilateral first intersection 4W	48.1	95.2	100
Augmented PI equilateral first intersection 160W	79.6	99.4	100
Augmented PI equilateral all intersections 4W	71.8	96.4	100
Augmented PI equilateral all intersections 160W	88.9	99.3	100
Augmented PI isosceles first intersection 4W	17	86	100
Augmented PI isosceles first intersection 160W	32.4	91.7	100
Augmented PI isosceles all intersections 4W	35.3	88	100
Augmented PI isosceles all intersections 160W	49.4	91.6	100

The above table represents the level of confidence that a node can be located within charging radius up to and including the given step.

The original PI with charger EIRP of 4W obtained an adequate localization for charging only 44% of the time. Thus, alone it is not accurate enough for this purpose. The additional refined PI brought the accuracy to suitable levels. With charger EIRP of 160W the confidence level of PI alone almost doubles.

Augmented PI equilateral with only the first intersection tested increased the confidence level only marginally over original PI.

Augmented PI equilateral with all intersections tested increases the confidence level for the initial trajectory substantially, to 72% and 89% for 4W and 160E EIRP respectively.

Augmented PI isosceles achieves a confidence level for the initial trajectory of less than 50% in all cases.

6.4 Average localization results, EIRP = 4W

Type	*Located by initial trajectory*	*Located by refined PI*	*Located by spiral*	*Location trajectory distance (m)*	*Mean location error (m)*
PI (original)	44.2	52	3.8	8500.04	2.64
Augmented PI equilateral first intersection	48.1	47.1	4.8	8504.80	2.57
Augmented PI equilateral all intersections	71.8	24.6	3.6	8127.06	1.94
Augmented PI isosceles first intersection	17	69	14	18948.81	9.69
Augmented PI isosceles all intersections	35.3	52.7	12	17175.94	7.79

The Augmented PI equilateral does not show an improvement over the original PI when only the first intersection is tested. However, when using all intersections, over 50% more nodes are located by the initial trajectory. There is a reduction of about 5% in the location trajectory distance and of about 25% in the mean location error.

The PI isosceles has a poor location rate using either the first or all intersections. It also has over location trajectory distances over twice those of its equilateral counterparts. This indicates that the obtuse angles of the perpendiculars resulting from the acute angles of the traces produce few accurate estimates, requiring many refinement steps.

6.5 Average localization results, EIRP = 160W

Type	*Located by initial trajectory*	*Located by refined PI*	*Located by spiral*	*Location trajectory distance (m)*	*Mean location error (m)*
PI (original)	78	21	1	8212.95	2.63
Augmented PI equilateral first intersection	79.6	19.8	0.6	9503.27	2.58
Augmented PI equilateral all intersections	88.9	10.4	0.7	9267.88	2.24
Augmented PI isosceles first intersection	32.4	59.3	8.3	16588.42	9.50
Augmented PI isosceles all intersections	49.4	42.2	8.4	15572.55	7.93

Using charger ERP of 160W doubles the charging radius and quadruples the charging footprint. As expected, the count of location by initial trajectory is increased, particularly for the isosceles trajectory which has the lowest accuracy.

The location trajectory distance for the Augmented PI modes shows an increase of about 15% despite an increase in the initial trajectory location count. The reason is that the ToC algorithm which is used to reduce the charging footprint travels more distance over a given area than the RSSI triangulation. Increasing the charging footprint makes it easier to find, i.e. produces more successes for the initial RSSI triangulation at the expense of increased total travel as more steps are executed within the charging footprint.

The increase in charger EIRP to 160W reduces the location trajectory distance for the isosceles modes by about 10%, but it is still almost double the other modes.

From the above it can be seen that the higher charger EIRP does not produce an improvement in localization efficiency with the algorithms used.

Chapter 7: Future Work

The following enhancements were considered to improve RSSI and ToC localization respectively but were not implemented.

7.1 Connectivity Qualification for RSSI Localization

Use connectivity graph (as produced by generateD) to qualify estimated positions. An estimated position can be eliminated if too far from a connected node which has already been located, reducing UAV travel.

7.2 Multiple Node ToC Localization

Generalize charging footprint trisection algorithm to handle situations when more than one node lies within charging footprint. This would allow multiple localizations from one RSSI based estimate, reducing UAV travel.

Appendices

Appendix A – Matlab Modules from Computational Optimization Laboratory [5]

A.1 test5-100.mat

This data file defines the node coordinates of the WSN for all simulations.

A.2 ESDP.p

This program file contains code for performing the cooperative localization simulations only.

A.3 SeDuMi 1.3

This directory contains program files for performing semidefinite optimization required by ESDP.p.

A.4 generateD.p

This program file generates the connectivity graph for the WSN with log-normal fading. It is called by the PI localization simulations, but the connectivity graph is not currently used.

Appendix B - Matlab Source

This appendix lists the Matlab program source code used to perform the simulations.

They can be found on GitHub, user @paul-durham.

B.1 ESDPrun.m

Main program for cooperative localization simulations.

B.2 pitile.m

Main program for original PI simulations.

B.3 pong.m

Main program for augmented PI simulations.

B.4 PIscan.m

B.5 PIscan1.m

B.6 PIscanP.m

B.7 LCscan.m

B.8 GetIntersect.m

B.9 Intersect.m

B.10 IntersectP.m

B.11 circlereduce.m

B.12 TOClocate3.m

B.13 TOCscan.m

B.14 UAVmove.m

Appendix C - Java Source

This appendix lists the Java program source code used to support the augmented PI simulations. It can be found on GitHub, user @paul-durham.

C.1 WSNode.java

References

[1] Boukerche, Azzedine, Horacio ABF Oliveira, Eduardo F. Nakamura, and Antonio AF Loureiro. "Localization systems for wireless sensor networks." *IEEE wireless Communications* 14, no. 6 (2007): 6-12.

[2] Chowdhury, Tashnim JS, Colin Elkin, Vijay Devabhaktuni, Danda B. Rawat, and Jared Oluoch. "Advances on localization techniques for wireless sensor networks: A survey." *Computer Networks* 110 (2016): 284-305.

[3] Patwari, Neal, Joshua N. Ash, Spyros Kyperountas, Alfred O. Hero, Randolph L. Moses, and Neiyer S. Correal. "Locating the nodes: cooperative localization in wireless sensor networks." *IEEE Signal processing magazine* 22, no. 4 (2005): 54-69.

[4] Biswas, Pratik, T-C. Liang, K-C. Toh, Yinyu Ye, and T-C. Wang. "Semidefinite programming approaches for sensor network localization with noisy distance measurements." *IEEE transactions on automation science and engineering* 3, no. 4 (2006): 360-371.

[5] Yinyu Ye, "Computational Optimization Laboratory," Accessed September 4, 2018. https://web.stanford.edu/~yyye/Col.html

[6] Guo, Zhongwen, Ying Guo, Feng Hong, Zongke Jin, Yuan He, Yuan Feng, and Yunhao Liu. "Perpendicular intersection: locating wireless sensors with mobile beacon." *IEEE Transactions on Vehicular Technology* 59, no. 7 (2010): 3501-3509.

[7] Sudevalayam, Sujesha, and Purushottam Kulkarni. "Energy harvesting sensor nodes: Survey and implications." *IEEE Communications Surveys & Tutorials* 13, no. 3 (2010): 443-461.

[8] Sample, Alanson P., Daniel J. Yeager, Pauline S. Powledge, Alexander V. Mamishev, and Joshua R. Smith. "Design of an RFID-based battery-free programmable sensing platform." *IEEE transactions on instrumentation and measurement* 57, no. 11 (2008): 2608-2615.

[9] Shu, Yuanchao, Peng Cheng, Yu Gu, Jiming Chen, and Tian He. "TOC: Localizing wireless rechargeable sensors with time of charge." *ACM Transactions on Sensor Networks (TOSN)* 11, no. 3 (2015): 44.

[10] Nikoletseas, Sotiris, Yuanyuan Yang, and Apostolos Georgiadis, eds. *Wireless power transfer algorithms, technologies and applications in ad hoc communication networks*. Springer, 2016.

[11] Ko, Ren-Song. "The complexity of the minimum sensor cover problem with unit-disk sensing regions over a connected monitored region." *International Journal of Distributed Sensor Networks* 8, no. 1 (2011): 918252.

[12] Tian, Di, and Nicolas D. Georganas. "A node scheduling scheme for energy conservation in large wireless sensor networks." *Wireless Communications and Mobile Computing* 3, no. 2 (2003): 271-290.

[13] Elliot, Robert S. *Antenna theory and design*. John Wiley & Sons, 2006. Chapter 2.

[14] Rappaport, T.S. *Wireless communications: principles and practice.* Prentice Hall, 2013. Chapter 4.